Improved performance of an FMX truck by normal force estimation and control

Master's thesis in Systems, Control and Mechatronics

AHMET ARIKAN

YUSUF TALHA BEKAROGLU

Department of Electrical Engineering
CHALMERS UNIVERSITY OF TECHNOLOGY
Gothenburg, Sweden 2018

MASTER'S THESIS 2018:EX053

Improved performance of an FMX truck by normal force estimation and control

AHMET ARIKAN
YUSUF TALHA BEKAROGLU

Department of Electrical Engineering
Division of Systems and Control
CHALMERS UNIVERSITY OF TECHNOLOGY
Gothenburg, Sweden 2018

Improved performance of an FMX truck by normal force estimation and control
AHMET ARIKAN, YUSUF TALHA BEKAROGLU

Supervisors: Leon Hendersson & Leo Laine, Volvo Group Trucks Technology, Gothenburg, Sweden
Examiner: Jonas Fredriksson, Department of Electrical Engineering, Chalmers University of Technology, Gothenburg, Sweden

Master's Thesis 2018:EX053
Department of Electrical Engineering
Division of Systems and Control
Chalmers University of Technology
SE-412 96 Gothenburg
Telephone + 46 (0)31-772 1000

Typeset in LaTeX
Gothenburg, Sweden 2018

Improved performance of an FMX truck by normal force estimation and control
AHMET ARIKAN
YUSUF TALHA BEKAROGLU
Department of Electrical Engineering
Chalmers University of Technology

Abstract:

During critical scenarios, such as hard straight-line braking and braking in a turn, handling of heavy vehicles demands improved subsystems for better performance and safety. The braking performance can be the difference between life and death in given scenarios. Within this thesis, firstly an estimation algorithm for estimating the normal forces on each wheel of a truck is developed Secondly, a linear spring suspension model is modified and made nonlinear to better represent a controllable air suspension system. Lastly, a controller based on control allocation for improved control global forces on x-, and y-direction and moment around x-, y-, and z-direction is developed. The proposed estimation and control algorithms are tested and verified by simulating the algorithms with mainly two test scenarios, hard straight-line braking and hard braking during steering. Simulations show the potential of the proposed system, i.e. the normal force estimator and the controller.

Keywords: control allocation, two-track model, normal force estimation

Acknowledgements

This master's thesis is carried out at the department of Suspension and Braking, at Volvo Group Trucks Technology (GTT) in Gothenburg.

We would like to begin by thanking our supervisors at GTT, Leon Henderson and Leo Laine, and our supervisor at Chalmers University of Technology, Jonas Fredriksson, for their support and perspective widening discussions throughout the thesis. We would also like to thank Bengt J H Jacobson, Sachin Janardhanan, Vincent Andreasson, and Zhetong Mo for their contribution to the thesis.

Last but not least, we would like to thank all of our friends and family for support and motivation.

Ahmet Arikan and Yusuf Talha Bekaroglu

Gothenburg, June 2018

Contents

List of Figures **ix**

1 Introduction **1**
1.1 Background . . . 1
1.1.1 Related work . . . 1
1.2 Purpose . . . 2
1.3 Scope . . . 2
1.4 Test Scenarios . . . 2
1.4.1 Straight-line braking . . . 2
1.4.2 Brake-in-turn maneuver . . . 2
1.5 Contribution of the thesis . . . 3
1.6 Outline of the thesis . . . 3

2 Modeling **4**
2.1 Vehicle Dynamics . . . 4
2.2 Normal Load . . . 7
2.2.1 Method 1 . . . 8
2.2.2 Static load . . . 9
2.2.3 Load transfer due to longitudinal and lateral acceleration 9
2.3 Suspension . . . 10

3 Estimator Design and Simulation **13**
3.1 Estimation Background . . . 13
3.2 Basic Normal Load Estimation . . . 13
3.3 Simulation Results . . . 14
3.3.1 VTM . . . 14
3.3.2 Test cases for estimation of normal load forces . . . 14
3.3.3 Soft straight-line braking . . . 15
3.3.4 Hard straight-line braking . . . 17
3.3.5 Soft steered braking . . . 19
3.3.6 Hard steered braking . . . 21

4 Control Theory and Design **24**
4.1 Control Theory . . . 24
4.2 Control Allocation . . . 24
4.2.1 Background . . . 24
4.2.2 Optimization . . . 26
4.3 Controller Design . . . 26
4.3.1 Background of control allocation in vehicle application . . 27
4.3.2 Pitch control . . . 27
4.3.3 Roll control . . . 28
4.3.4 Pitch and roll control . . . 29
4.3.5 Constraints . . . 29
4.4 Control Allocator Simulation . . . 30

4.4.1 Test cases for the control allocator 31
4.4.2 Hard straight-line braking pitch control 31
4.4.3 Hard straight-line braking pitch control ideal 33
4.4.4 Hard straight-line braking combined pitch & roll control . 36
4.4.5 Steered hard braking roll control 38
4.4.6 Steered hard braking roll control ideal 40
4.4.7 Steered hard braking combined pitch & roll control 42
4.4.8 Steered hard braking combined pitch & roll control ideal . 44
4.4.9 Steered hard braking combined pitch & roll control ideal 120% P˙max 47
4.5 Modified Control Allocator Simulation 49
4.5.1 Steered hard braking combined pitch & roll control 49

5 Conclusion **51**
5.1 Discussion 51
5.2 Future Work 51
5.2.1 Estimation 51
5.2.2 Actuator models 52

6 Bibliography **53**

References **53**

7 Appendix **II**
7.1 Noisy Data Simulation in VTM II
7.1.1 Noisy data simulation for Method 1 soft straight-line braking II
7.1.2 Noisy data simulation for Method 1 hard straight-line braking II
7.1.3 Noisy data simulation for Method 1 soft steering braking III
7.1.4 Noisy data simulation for Method 1 hard steering braking IV

List of Figures

2.1 Figure shows coordinate axes of a vehicle and sketch of a vehicle, [1] 4
2.2 Force definitions, lengths, widths and coordinate system of the truck is shown in the figure. The first axle is steering axle, second and third axles are driven axles of the truck. E_1, E_2 and E_3 represents the width of the axles respectively first, second and third axles. l_1, l_2 and l_3 are distance from axles to center of gravity. The tag axle is considered as lifted. 6
2.3 Figure shows control structure of the bellow 12
3.1 Structure of basic estimation 14
3.2 Acceleration in x-, y- and z-direction during soft straight-line braking 15
3.3 Scenario: Soft straight-line Braking - Estimation of normal load forces on each wheel (blue line) compared to the normal load forces on each wheel from the VTM (red line) 16
3.4 Scenario: Soft straight-line Braking - Estimation of normal load forces on each wheel (blue line) compared to the normal load forces on each wheel from the VTM (red line) 16
3.5 Acceleration in x-, y- and z-direction during hard straight-line braking 17
3.6 Scenario: Hard straight-line braking - Estimation of normal load forces on each wheel (blue line) compared to the normal load forces on each wheel from the VTM (red line) 18
3.7 Scenario: Hard straight-line braking - Estimation of normal load forces on each wheel (blue line) compared to the normal load forces on each wheel from the VTM (red line) 18
3.8 Acceleration in x-, y- and z-direction during steered braking . . . 19
3.9 Scenario: Soft Steered Braking - Estimation of normal load forces on each wheel (blue line) compared to the normal load forces on each wheel from the VTM (red line) 20
3.10 Scenario: Soft Steered Braking - Estimation of normal load forces on each wheel (blue line) compared to the normal load forces on each wheel from the VTM (red line) 20
3.11 Acceleration in x-, y- and z-direction during steered braking . . . 21
3.12 Scenario: Hard Steered Braking - Estimation of normal load forces on each wheel (blue line) compared to the normal load forces on each wheel from the VTM (red line) 22
3.13 Scenario: Hard Steered Braking - Estimation of normal load forces on each wheel (blue line) compared to the normal load forces on each wheel from the VTM (red line) 22
4.1 Control allocation structure is presented [1]. 25
4.2 Acceleration in x- and y-direction during hard straight-line braking 31
4.3 Roll and Pitch angles 32
4.4 Requested suspension pressure 33
4.5 Achieved suspension pressure 33

4.6 Requested suspension pressure 34
4.7 Achieved suspension pressure 34
4.8 Acceleration in x- and y-direction during hard straight-line braking 35
4.9 Roll and Pitch angles 35
4.10 Acceleration in x- and y-direction during steered hard braking . . 36
4.11 Roll and Pitch angles 37
4.12 Requested suspension pressure 37
4.13 Achieved suspension pressure 38
4.14 Acceleration in x- and y-direction during steered hard braking . . 38
4.15 Roll and Pitch angles 39
4.16 Requested suspension pressure 39
4.17 Achieved suspension pressure 40
4.18 Requested suspension pressure 40
4.19 Achieved suspension pressure 41
4.20 Acceleration in x- and y-direction during steered hard braking . . 41
4.21 Roll and Pitch angles 42
4.22 Acceleration in x- and y-direction during steered hard braking . . 42
4.23 Roll and Pitch angles 43
4.24 Requested suspension pressure 44
4.25 Achieved suspension pressure 44
4.26 Requested suspension pressure 45
4.27 Achieved suspension pressure 45
4.28 Acceleration in x- and y-direction during steered hard braking . . 46
4.29 Roll and Pitch angles 46
4.30 Requested suspension pressure 47
4.31 Achieved suspension pressure 47
4.32 Acceleration in x- and y-direction during steered hard braking . . 48
4.33 Roll and Pitch angles 48
4.34 Acceleration in x- and y-direction during steered hard braking . . 49
4.35 Roll and Pitch angles 49
4.36 Requested suspension pressure 50
4.37 Achieved suspension pressure 50
5.1 Scenario:Steered hard braking - Normal load forces on each wheel compared to sensor on every tyre (blue signal with dash) compared to the VTM model (red signal) 52
7.1 Scenario: Soft Line Braking - Estimation of normal load forces on each wheel (blue line) compared to the normal load forces on each wheel from the VTM (red line) and filtered estimation of normal load forces on each wheel (green line) II
7.2 Scenario: Hard Line Braking - Estimation of normal load forces on each wheel (blue line) with compared to the load forces on each wheel from the VTM (red line) and filtered estimation of normal load forces on each wheel (green line) III

7.3 Scenario: Soft Turn Braking - Estimation of normal load forces on each wheel (blue line) compared to the normal load forces on each wheel from the VTM (red line) and filtered estimation of normal load forces on each wheel (green line) IV
7.4 Scenario: Hard Turn Braking - Estimation of normal load forces on each wheel (blue line) with compared to the load forces on each wheel from the VTM (red line) and filtered estimation of normal load forces on each wheel (green line) IV

1 Introduction

This thesis aims to improve the braking and handing performance of a heavy vehicle by coordinating vertical suspension forces with other actuators on the vehicle. The following sections will present the background, purpose, scope, test scenarios and outline of the report.

1.1 Background

There are many different types of heavy vehicles used in different businesses which include transportation and construction. For example, transportation trucks are different from construction trucks in terms of chassis and suspension. Construction trucks have a stronger chassis compared to transportation trucks [1]. Transportation trucks are not built for gravel roads since their suspension is built for higher frequency vibrations, while construction truck suspensions are more complex and flexible, which makes traveling on gravel roads easier and more comfortable.

Typically, dynamic vertical tyre forces are not directly measured on modern heavy vehicles. Due to the different applications mentioned above, it is a challenge to design an estimator for heavy vehicles to control and improve the vehicle of motion. This estimator should not have any significant offsets to affect vehicle motion management system. Even though studies have been done about estimating normal forces, it is a still developing area. Industries will be able to reduce the number of sensors, thus the cost of the complete vehicle, by having good state estimators. Modern trucks often have electronically control air suspension, which enables suspensions properties to be adjusted in real-time.

This thesis focuses on improving driving automation of heavy vehicles by including normal force estimation on each wheel and designing a controller to manipulate the forces generated by the suspension system during braking a turning maneuvers to improve the stability of the vehicle.

1.1.1 Related work

From the literature it is found that studies investigating dynamic normal load estimation have mainly focused on two-axle vehicles. For example, the study [2] estimates vertical and lateral tyre forces considering the road angle and road irregularity for a two-axle vehicle. Another example, the study [3] estimates the lateral load transfer and normal load forces for a two-track model with two-axles. Moreover, in [4], a Kalman Filter was used to estimate forces on each wheel. Further, in [5], an Unscented Kalman Filter was used to estimate normal forces on each wheel, which was also used to calculate the truck angle. The article [6] explains estimation of the roll state of a truck. Similar to that, an Extended Kalman Filter is used to estimate the side-slip and wheel cornering stiffness of a truck in [7].

Control allocation is presented in [8] for flight applications. Furthermore, coordination of actuators in a heavy vehicle by using control allocation formulation is presented in [1].

1.2 Purpose

The purpose of the thesis is to gain insight into dynamics of an FMX[1] truck and to improve the performance of the vehicle in critical braking and handling situations such as straight-line braking or braking in a turn.

1.3 Scope

The scope of the thesis is limited to the following:

- Derive a two-track model of an FMX truck. The model will be used for estimation of normal forces on each wheel. The two-track model will include longitudinal, lateral and vertical dynamics.
- The normal load estimator will be validated using a high-fidelity simulation model of an FMX truck.
- Develop a controllable suspension model.
- Design of a controller for controlling pitch and roll moments of an FMX truck.

1.4 Test Scenarios

Testing the estimation and control algorithms will be done by two test scenarios. In this subsection, two main test scenarios are given.

1.4.1 Straight-line braking

In the straight-line braking scenario, the truck is tested with two different braking torques which are considered to represent soft straight-line braking and hard straight-line braking respectively. The truck has an initial speed in the x-direction and then starts to brake. The aim of the tests applied is to verify the longitudinal load transfer of the truck. The road tyre friction coefficient is considered to be $\mu = 1$, which is representative of a dry road.

1.4.2 Brake-in-turn maneuver

In the brake-it-turn scenario, the truck is tested when it is doing a cornering maneuver while braking. The truck has an initial speed in the x-direction, a fixed steering angle, and after a few seconds starts to brake. Braking is done with two different decelerations. One of them is considered as hard braking,

[1] An FMX truck is a Volvo specific model, it as a single unit vehicle which can have a gross weight up to 24 tonne, designed for off-road applications (e.g. construction sites).

and the other one is soft braking. This test aims to verify that the estimation algorithms can accurately estimate the longitudinal and lateral load transfer of the truck. The road tyre friction coefficient is considered to be $\mu = 1$, which is a dry road.

1.5 Contribution of the thesis

Benefits of the thesis are that to reduce roll and pitch angles during cornering and braking maneuvers, and that this has potential to reduce the chance of vehicle roll over, improve vehicle stability and potentially reduce stopping distance when a truck is braking in a straight-line or in-turn maneuver. Practically, these features developed are highly beneficial in real life.

1.6 Outline of the thesis

The remainder of the thesis is presented as follows: Chapter 2: a two-track model is derived for an FMX truck. The chapter also describe suspension dynamics. Chapter 3: a dynamic normal force estimator is presented and validated using simulation. In chapter 4 control allocation theory and design is described and an existing control allocator for a heavy vehicle is extended to include pitch and roll motion. Results of control allocation simulations are also presented. In chapter 5 conclusions of the thesis and future work ideas are stated.

2 Modeling

To estimate normal load forces on each wheel and to design a suspension controller for a truck, a vehicle dynamics model needs to be derived. In this chapter, first, the equations of motions are derived. In the next section, normal load force equations are presented. Lastly, the air suspension model is defined [9]. For this thesis, an FMX truck is considered. The FMX truck has a 8x4 configuration (4 axels and 8 wheels), but in the modelling the last axel, also known as 'tag axel', is lifted. Hence, only 3 axels and 6 wheels are considered.

2.1 Vehicle Dynamics

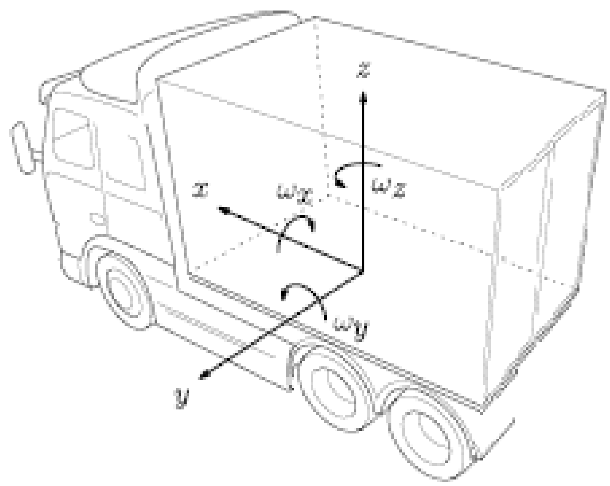

Figure 2.1: Figure shows coordinate axes of a vehicle and sketch of a vehicle, [1]

The FMX truck is studied in this work. It is referred to as a 6x4 truck, or 8x4 with lifted tag axle, as mentioned in earlier. The truck has one steering axle and two driven axles.

The model presented is only used for the normal load estimation algorithm and not used for complete vehicle system simulation. For complete vehicle system simulations, the Volvo Transportation Model (VTM) is used [9].

The equations of motion in x-, y- and z-direction are derived accordingly to [10], as:

$$m * (a_x) = \sum F_x \tag{1}$$

$$m * (a_y) = \sum F_y \tag{2}$$

$$I_z * \dot{w}_z = \sum F_{y,i} * l_i + \sum F_{x,i} * \frac{E_i}{2} \tag{3}$$

where m is total mass of the truck, a_x is the longitudinal acceleration of the truck, a_y is the lateral acceleration of the truck, w_z is the yaw rate, F_x and F_y are the longitudinal and lateral forces, l_i is the longitudinal distance of each axle to the center of gravity of the truck where $i = 1, 2, 3$ represents the first, second and third axle. E_i is the width where $i = 1, 2, 3$ represents the first, second and third axle. I_z is inertia of truck in x- and z-direction. The coordinate axes are defined as in Figure 2.1 and Figure 2.2.

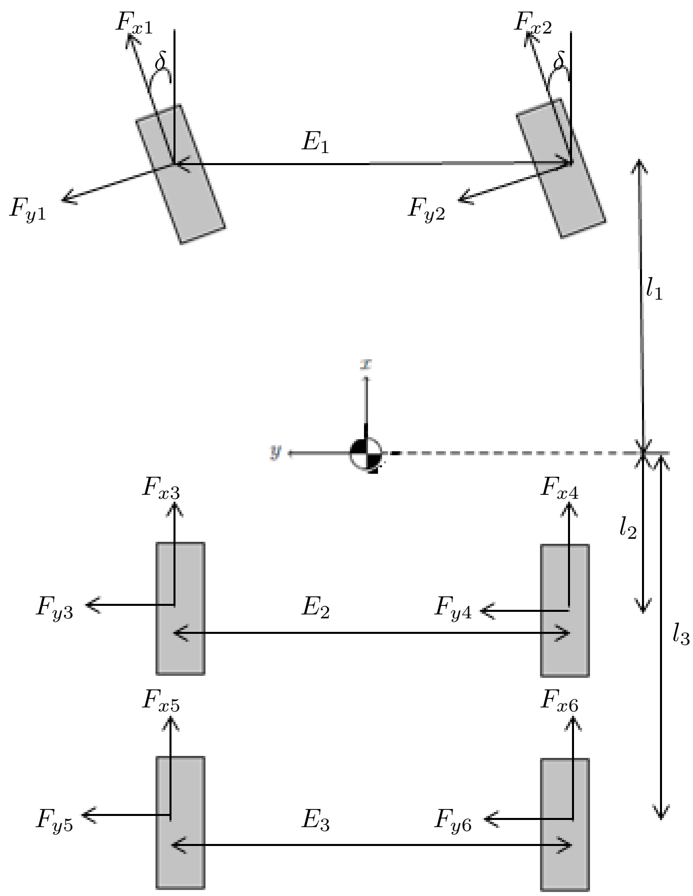

Figure 2.2: Force definitions, lengths, widths and coordinate system of the truck is shown in the figure. The first axle is steering axle, second and third axles are driven axles of the truck. E_1, E_2 and E_3 represents the width of the axles respectively first, second and third axles. l_1, l_2 and l_3 are distance from axles to center of gravity. The tag axle is considered as lifted.

The equations of motion for this vehicle is represented in equation 4, 5 and 6. Yaw acceleration has been neglected to make more simple in these equations.

The longitudinal forces are:

$$\begin{aligned}\sum F_x =&(F_{x1} * cos(\delta) - F_{y1} * sin(\delta)) + (F_{x2} * cos(\delta) - \cdots \\ &\cdots F_{y2} * sin(\delta)) + F_{x3} + F_{x4} + F_{x5} + F_{x6}\end{aligned} \tag{4}$$

where $F_{x,i}$, $i = 1, 2$, represents the front wheel longitudinal forces respectively left tyre and right tyre, $F_{x,i}$, $i = 3, 4, 5, 6$ represent rear axles longitudinal forces. The lateral forces effecting the vehicle are:

$$\begin{aligned}\sum F_y =& - (F_{x1} * sin(\delta) - F_{y1} * cos(\delta)) - (F_{x2} * sin(\delta) - \cdots \\ &\cdots F_{y2} * cos(\delta)) + F_3 + F_{y4} + F_{y5} + F_{y6}\end{aligned} \tag{5}$$

where $F_{y,i}$, $i = 1, 2$, represents the front wheels lateral forces respectively left tyre and right tyre, and $F_{y,i}$, $i = 3, 4, 5, 6$ represent rear axles lateral forces. The lateral and longitudinal forces also create a yaw moment as:

$$\begin{aligned}\sum F_{y,i} * l_i + \sum F_{x,i} * \frac{E_i}{2} =& - (F_{x1} * sin(\delta) + F_{y1} * cos(\delta) + F_{x2} * sin(\delta) + \cdots \\ &\cdots F_{y2} * cos(\delta)) * l_1 - (F_{y3} + F_{y4}) * l_2 - \cdots \\ &\cdots (F_{y5} + F_{y6}) * l_3 + (F_{x1} * cos(\delta) - F_{y1} * sin(\delta) + \cdots \\ &\cdots F_{x3} + F_{x5}) * \frac{E_3}{2} - (F_{x2} * cos(\delta) - \cdots \\ &\cdots F_{y2} * sin(\delta) + F_{x4} + F_{x6}) * \frac{E_3}{2}\end{aligned} \tag{6}$$

where E_i is the width of the truck and the truck has equal width in all axes. The pitch torque is determined as:

$$\sum M_x = (m * g * h_{cg}) - K_r * \phi - C_r * \dot{\phi} \tag{7}$$

where g is the gravitational acceleration, ϕ is the relative angle between the road/axle and the vehicle's mass, h_{cg} is the height of the center of gravity of the truck, K_r is rotational stiffness and C_r is damping coefficient.

2.2 Normal Load

The vehicle's normal load distribution is the central part of the modeling chapter. To develop a normal load force estimator for a 6x4 truck, a method is investigated. A method is developed from [2], which will be called Method 1 from now on. Method 1 includes the affects of roll and pitch, and vertical acceleration. The effects of load transfer (from longitudinal and lateral acceleration) are handled separately in sections 2.2.2 and 2.2.3.

2.2.1 Method 1

In [2], the two-track model is derived for a two-axle vehicle. In this thesis, a truck with 3 axles is considered. Hence, these equations are modified. Equations for a vehicle with two axles are given below, from [2].

$$M_\theta = K_p\theta + C_p\dot{\theta} \tag{8}$$

$$M_\phi = K_r\phi + C_r\dot{\phi} \tag{9}$$

where M_θ is the pitch moment of the truck, M_ϕ is the roll moment of the truck, K_p and C_p are coefficient for pitch movement, K_r and C_r are coefficient for roll moment. Below equation defines the normal force changes on a tyre as:

$$F_{z11} = \frac{ml_2a_z}{2l} - \frac{l_2(K_p\theta + C_p\dot{\theta})}{lE_1} + \frac{K_r\phi + C_r\dot{\phi}}{2l} - \frac{M_\theta M_\phi}{ma_zlE_1} \tag{10}$$

where l_2 is length which is from the second axle to center of gravity of the vehicle, l is the wheelbase length, E_1 is width of front axle. F_{zij}, $i = 1, 2$ represents the axles, $j = 1, 2$ represents left and right wheels, is the vertical forces on each wheel.

$$F_{z12} = \frac{ml_2a_z}{2l} + \frac{l_2(K_p\theta + C_p\dot{\theta})}{LE_1} + \frac{K_r\phi + C_r\dot{\phi}}{2l} + \frac{M_\theta M_\phi}{ma_zlE_1} \tag{11}$$

$$F_{z21} = \frac{ml_1a_z}{2l} - \frac{l_1(K_p\theta + C_p\dot{\theta})}{lE_2} - \frac{K_r\phi + C_r\dot{\phi}}{2l} + \frac{M_\theta M_\phi}{ma_zlE_2} \tag{12}$$

$$F_{z22} = \frac{ml_1a_z}{2l} + \frac{l_1(K_p\theta + C_p\dot{\theta})}{lE_2} - \frac{K_r\phi + C_r\dot{\phi}}{2l} - \frac{M_\theta M_\phi}{ma_zlE_2} \tag{13}$$

where l_1 is the length which is from the first axle to center of gravity of the vehicle, E_2 is the width of the rear axle.

The first step is to split the forces, which is done by applying mass per axle on the normal load force equations and not total mass. The equations which are 10, 11, 12 and 13 are modified.

$$F_{z11} = \frac{m*(l-l_1)*a_z}{2*l} - \frac{(l-l_1)*(K_r*\phi + C_r*\dot{\phi})}{l*E_1} + \frac{K_p*\theta + C_p*\dot{\theta}}{2*l} - \frac{M_\theta*M_\phi}{m*a_z*l*E_1} \tag{14}$$

$$F_{z12} = \frac{m*(l-l_1)*a_z}{2*l} + \frac{(l-l_1)*(K_r*\phi + C_r*\dot{\phi})}{l*E_1} + \frac{K_p*\theta + C_p*\dot{\theta}}{2*l} + \frac{M_\theta*M_\phi}{m*a_z*l*E_1} \tag{15}$$

$$F_{z21} = \frac{m*(l-l_2)*a_z}{2*l} - \frac{(l-l_2)*(K_r*\phi + C_r*\dot{\phi})}{l*E_2} - \frac{K_p*\theta + C_p*\dot{\theta}}{2*l} + \frac{M_\theta*M_\phi}{m*a_z*l*E_2} \tag{16}$$

$$F_{z22} = \frac{m*(l-l_2)*a_z}{2*l} + \frac{(l-l_2)*(K_r*\phi + C_r*\dot{\phi})}{l*E_2} - \frac{K_p*\theta + C_p*\dot{\theta}}{2*l} - \frac{M_\theta*M_\phi}{m*a_z*l*E_2} \tag{17}$$

$$F_{z31} = \frac{m*(l-l_3)*a_z}{2*l} - \frac{(l-l_3)*(K_r*\phi + C_r*\dot{\phi})}{l*E_3} - \frac{K_p*\theta + C_p*\dot{\theta}}{2*l} + \frac{M_\theta * M_\phi}{m*a_z*l*E_3} \tag{18}$$

$$F_{z32} = \frac{m*(l-l_3)*a_z}{2*l} + \frac{(l-l_3)*(K_r*\phi + C_r*\dot{\phi})}{l*E_3} - \frac{K_p*\theta + C_p*\dot{\theta}}{2*l} - \frac{M_\theta * M_\phi}{m*a_z*l*E_3} \tag{19}$$

where l_3 is the length which is from the third axle to center of gravity of the vehicle, E_3 is the width of the rear axle, and l is the distance between the first and rear-most axle. These equations are for 6x4 a truck.

2.2.2 Static load

The static load, which is the load when the truck is standing still, is defined as:

$$F_{zij} = \frac{m_{axle_i} * g}{2} \tag{20}$$

where i and j denotes the number of axle and wheel and m_{axle_i} presents the load on each axle.

2.2.3 Load transfer due to longitudinal and lateral acceleration

When the truck brakes or turns, it will have accelerations in x-, y- and z-directions. The longitudinal tyre forces on a truck (or car) typically do not act through the vehicle's centre of mass. During longitudinal and lateral acceleration an opposing moment must therefor be generated by the tyre vertical forces. This change in vertical tyre force due to these effects are expressed in equations 14-19. The equations in Method 1 has to consider these changes. Adding longitudinal and lateral load transfers in the model make the result more accurate. The longitudinal load transfer has been taken from the existing Volvo load transfer model, presented in equations 21-26 while the lateral load transfer has been derived from a two-axle vehicle and later modified (see equations 27-32).

$$F_{z11} = -\frac{1}{2} * \frac{h_{cg}*m*ax}{(a+b)} \tag{21}$$

$$F_{z12} = -\frac{1}{2} * \frac{h_{cg}*m*ax}{(a+b)} \tag{22}$$

$$F_{z21} = \frac{1}{2} * \frac{h_{cg}*m*ax}{a+b} * \frac{b_{D1}}{b_{D1}+b_{D2}} \tag{23}$$

$$F_{z22} = \frac{1}{2} * \frac{h_{cg}*m*ax}{a+b} * \frac{b_{D1}}{b_{D1}+b_{D2}} \tag{24}$$

$$F_{z31} = \frac{1}{2} * \frac{h_{cg}*m*ax}{a+b} * \frac{b_{D2}}{b_{D1}+b_{D2}} \tag{25}$$

$$F_{z32} = \frac{1}{2} * \frac{h_{cg} * m * ax}{a+b} * \frac{b_{D2}}{b_{D1} + b_{D2}} \tag{26}$$

where l_1 meters is the longitudinal distance from the front axle to center of gravity of the truck, l_2 is longitudinal distance from the first drive axle to center of gravity of the truck, and l_3 is longitudinal distance from the second drive axle to center of gravity of the truck, and finally $b = \frac{l_2+l_3}{2}$ is averaged longitudinal distance of the drive to center of gravity of the truck. The lateral load transfer per front wheel is:

$$F_{z11} = -\frac{1}{E_1}\frac{m_{axle1}}{2} * a_y * h_{cg} * \frac{l - l_1}{l} \tag{27}$$

$$F_{z12} = \frac{1}{E_1}\frac{m_{axle1}}{2} * a_y * h_{cg} * \frac{l - l_1}{l} \tag{28}$$

$$F_{z21} = -\frac{1}{E_2}\frac{m_{axle2}}{2} * a_y * h_{cg} * \frac{l + l_2}{l} \tag{29}$$

$$F_{z22} = \frac{1}{E_2}\frac{m_{axle2}}{2} * a_y * h_{cg} * \frac{l + l_2}{l} \tag{30}$$

$$F_{z31} = -\frac{1}{E_3}\frac{m_{axle3}}{2} * a_y * h_{cg} * \frac{l + l_3}{l} \tag{31}$$

$$F_{z32} = \frac{1}{E_3}\frac{m_{axle3}}{3} * a_y * h_{cg} * \frac{l + l_3}{l} \tag{32}$$

The denominator for mass is the number of wheels and has hence been modified for the FMX Truck. The lengths has been chosen as l_2 when calculating forces for the second axle and as l_3 when calculating forces on the third axle.

Equations 14-19, equation 20, equations 21-26 and equations 27-32 are added to find the total vertical forces on each wheel. Equation 14-19 considers the change in roll and pitch angles. Equation 20 considers the static load on each axle. Equations 21-26 consider the longitudinal load transfer in the x-direction. Equations 27-32 consider the lateral load transfer in the y-direction.

2.3 Suspension

Suspension is modeled as combination of a damper and a spring. The equations 14, 15, 16, 17, 18 and 19 have suspension terms: $(K_r * \phi + C_r * \dot{\phi})$ and $(K_p * \theta + C_p * \dot{\theta})$. In this work, these equations are replaced with an active suspension actuator.

The actuator works as follow. The simple spring is replaced with an air bellow with flowrate. The flow rate of air into (and out of) the air bellow can be used to adjust its stiffness characteristics. The pressure of one bellow equation is calculated as:

$$P = \frac{\int q}{A * z + DriveLevelVolume} \tag{33}$$

where A is the area of the bellow in m^2, z is the height change in m, *Driver-LevelVolume* is the initial area in a bellow in m^3 and q is the air flowrate in m^3/s.

The equation for the left and right bellows are the same, but the flowrate is given by the controller and does vary. Left and right pressures are added. Since the stiffness can increase and decrease after this modification, the height of the joints could also reach unreasonably height limits. Hence, a bumpstop has been added to the model which purpose is to limit of the suspension bellow height.

Since it is an air suspension and the valves are not ideal, the suspension does not reach the airflow limits instantly but have time delays due to dynamics of the system. The equations for the flowrate has been derived and taken from [11].

$$\dot{m_v} = \begin{cases} S_v * C_f * A_v * C_1 * \frac{P_u}{\sqrt{T_{cham}}}, & \frac{P_d}{P_u} \leq p_{cr} \\ S_v * C_f * A_v * C_2 * \frac{P_u}{\sqrt{T_{cham}}} * \frac{P_d}{P_u}^{\frac{1}{\gamma}} * \sqrt{1 - \frac{P_d}{P_u}^{\frac{\gamma-1}{\gamma}}}, & \frac{P_d}{P_u} > p_{cr} \end{cases} \tag{34}$$

where v stands for 'valve' and can be either an inlet or outlet, C_f is the valve discharge coefficient, A_v is the valve orifice cross-sectional area, P_u is the up-stream pressure, and P_d is the downstream pressure. C_1 and C_2 are constants defined by:

$$C_1 = \sqrt{\frac{\gamma}{R} * (\frac{2}{\gamma + 1})^{\frac{\gamma+1}{\gamma - 1}}} \tag{35}$$

$$C_2 = \sqrt{\frac{2 * \gamma}{R * (\gamma - 1)}} \tag{36}$$

p_{cr} is the critical pressure ratio, and is calculated by:

$$p_{cr} = (\frac{2}{\gamma + 1})^{\frac{\gamma}{\gamma - 1}} \tag{37}$$

The pressure request from the controller is sent into a pressure error control which takes the difference of the current bellow pressure and the desired, puts it through a deadzone and sends it into the flowrate model. The control structure of the pressure controller is given in figure 2.3.

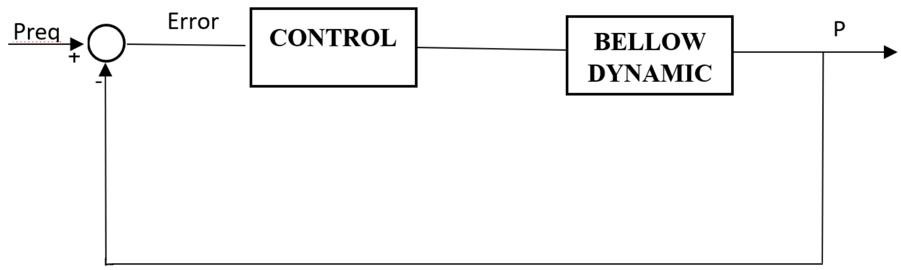

Figure 2.3: Figure shows control structure of the bellow

3 Estimator Design and Simulation

The following chapter will present the estimation design for normal force on each wheels. Firstly, the background of estimators is presented. Secondly, the basic estimation structure for normal force estimation is explained. Simulation results which are compared with the VTM is given in the last section.

3.1 Estimation Background

Estimation is needed in the vehicle industry recently, since measuring all states of the vehicle with sensors is costly. Estimation techniques are used in the automotive industry to improve from active safety, autonomous driving and drive comfort.

In literature, there are two general types of estimators. These are open loop estimator and closed loop estimator. Open loop estimators work without feedback from the system. On the other hand, closed loop estimators have feedback in their models. Therefore, closed loop estimators are more accurate comparing the open loop estimators. There are many examples about closed loop estimators in literature [2], [3] and [4]. In one example, the vertical forces are estimated using a Linear Kalman filter, [2] where vehicle states are chosen as global accelerations, roll, pitch, roll rate, pitch rate and normal forces. The mathematical model of the vehicle derived is linear.

In this thesis, an open loop estimation algorithm is used for estimating the normal forces. Due to time constraints, closed loop estimation techniques are out of the scope of this thesis.

3.2 Basic Normal Load Estimation

An open loop estimator structure is chosen for this work because of complexity of the closed loop state vectors. In the future the open loop estimator developed here could be extended to a close loop form.

The basic estimation method is based on the sensor outputs from the vehicle system, where it is represented by the VTM in the thesis. The estimation block consists of the normal load force equations, which are given in the modeling section. The method structure is given in figure 3.1.

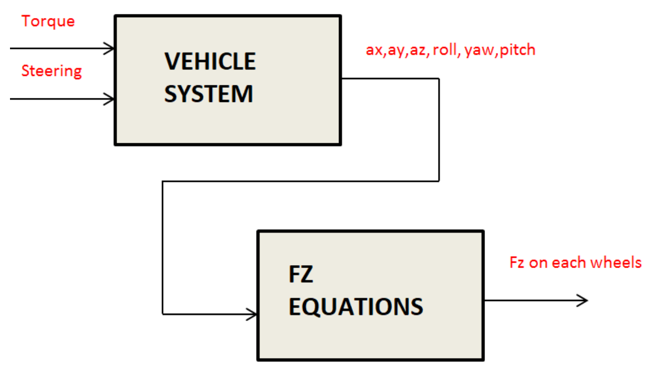

Figure 3.1: Structure of basic estimation

The inputs of the system are engine torque and steering angles. Estimation of normal load forces, according to the provided method equations in section 2, require global acceleration in x-, y- and z-direction, and roll, pitch and yaw angles as an input. Forces are calculated in "F_z equations" block. Method 1 (described in Section 2.2.1.) has been used to estimate the contribution from roll and pitch in the results presented here.

3.3 Simulation Results

The following section presents the Volvo Transport Model (VTM) as well as the cases for validating the estimation of normal load forces.

3.3.1 VTM

The Volvo Transport Model (VTM) is a simulation tool for heavy vehicles [9]. The VTM is developed in the Matlab/Simulink environment. In this work, the VTM has been physical models for the chassis and contains detailed vehicle dynamics. The VTM has been updated by adding an active suspension system which is defined in section 2.3.

The VTM provides simulated sensor data to the normal load force estimator and also provides measurements of the real normal load force. The comparison of the real data and the estimated data is carried out using on the VTM to verify the functionality of the derived equations. As mentioned above, the different test cases include testing different brake forces without any steering input and then braking while steering the vehicle.

3.3.2 Test cases for estimation of normal load forces

Estimation of normal load forces is tested in four different test scenarios: soft straight-line braking, hard straight-line braking, soft steered braking and hard steered braking.

In the straight-line braking, the truck will only have pitching motion due to no steering angle. The aim of this test is to observe the change in normal load force due to longitudinal load transfer in the x-direction. Giving a steering angle to the truck causes roll motion. The results of steered hard braking in straight-line will show the performance of the estimation algorithm regarding combined lateral and longitudinal load transfer.

The results from simulations are provided in this section, which is compared with simulation data from the VTM. In simulations, a dry road is chosen. The tyre-road coefficient value is $\mu = 1$. It is chosen as dry road to not activate the ABS in the VTM during the simulations.

3.3.3 Soft straight-line braking

Soft straight-line braking has $\sim$ -0.9 m/s^2 deceleration in a straight-line with zero degree steering input. Figure 3.2 shows acceleration changes in x-, y- and z-direction, during the soft straight-line braking. Due to braking, y- and z-direction have acceleration changes.

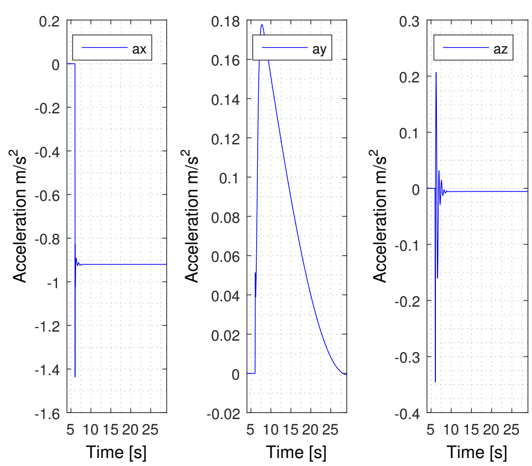

Figure 3.2: Acceleration in x-, y- and z-direction during soft straight-line braking

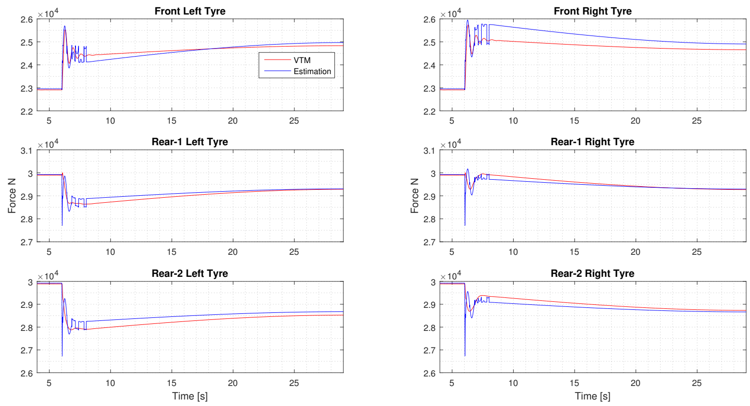

Figure 3.3: Scenario: Soft straight-line Braking - Estimation of normal load forces on each wheel (blue line) compared to the normal load forces on each wheel from the VTM (red line)

Figure 3.3 shows the normal load forces on each wheel. The estimator shows no significant offset compared to the VTM, which indicates that the estimation algorithm is working correctly. From figure 3.3, it can also be seen that the load of the front axle is increasing and the load on the rear axles are decreasing, which is reasonable. The oscillation in the beginning of the braking (at 6 seconds) is due to the initial acceleration in the z-direction.

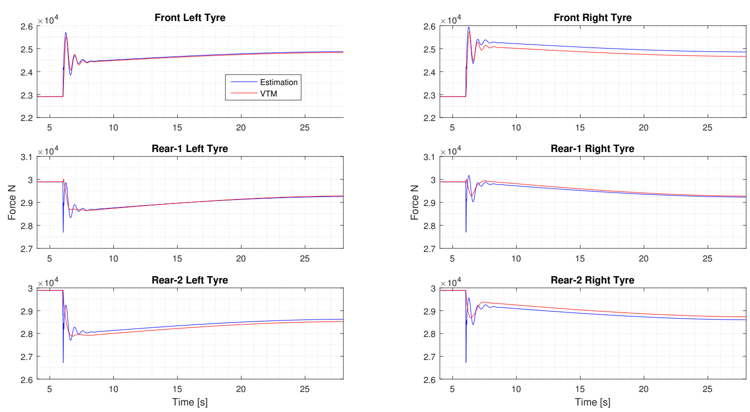

Figure 3.4: Scenario: Soft straight-line Braking - Estimation of normal load forces on each wheel (blue line) compared to the normal load forces on each wheel from the VTM (red line)

Estimator equations are modified by removing the a_z acceleration in denominator due to spikes and oscillations. Figure 3.4 shows the normal load forces on each wheel. In this way, estimator works more accurate compared to Figure 3.3.

3.3.4 Hard straight-line braking

Hard straight-line braking has a deceleration of 3 m/s^2 with zero degree steering input. This test is done to see that the pitching motion and the longitudinal load transfers are adequately estimated in the algorithm. Figure 3.5 shows acceleration changes for the vehicle.

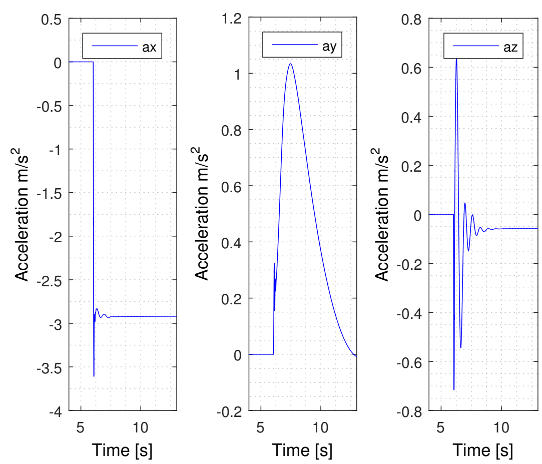

Figure 3.5: Acceleration in x-, y- and z-direction during hard straight-line braking

Figure 3.5 shows that truck has 3 m/s^2 deceleration in x-direction. Due to the initial speed of the truck being large, $22m/s$, and braking hard with a deceleration of with 3 m/s^2, it causes acceleration in the y-direction. When the truck has started braking, acceleration in y- and z-direction are also affected due to high-speed braking and normal load changes respectively.

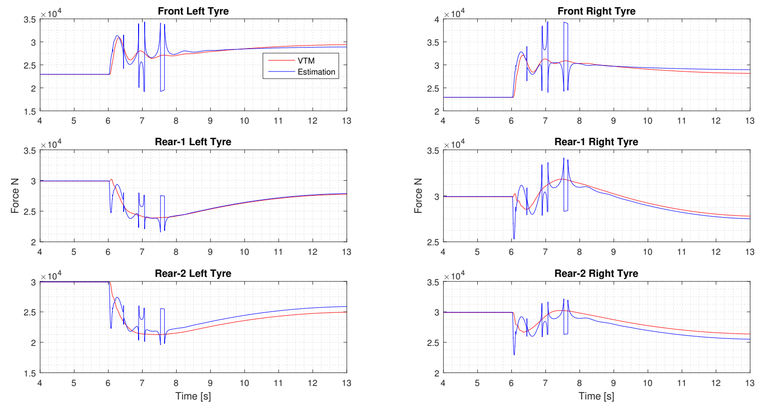

Figure 3.6: Scenario: Hard straight-line braking - Estimation of normal load forces on each wheel (blue line) compared to the normal load forces on each wheel from the VTM (red line)

Figure 3.6 shows the normal load forces on each wheel. The estimator shows no significant offset at steady-state compared to the VTM. From figure 3.6, it can also be seen that the load of the front axle is increased relative to the soft straight-line braking case which is around %40 percent change in per wheel and the load on the rear axles are decreasing which is around %20 percent change in per wheel, which is reasonable. The oscillation in the beginning of the braking (at 6 seconds) is due to the initial acceleration in the z-direction. The estimation results follow the VTM in steady state.

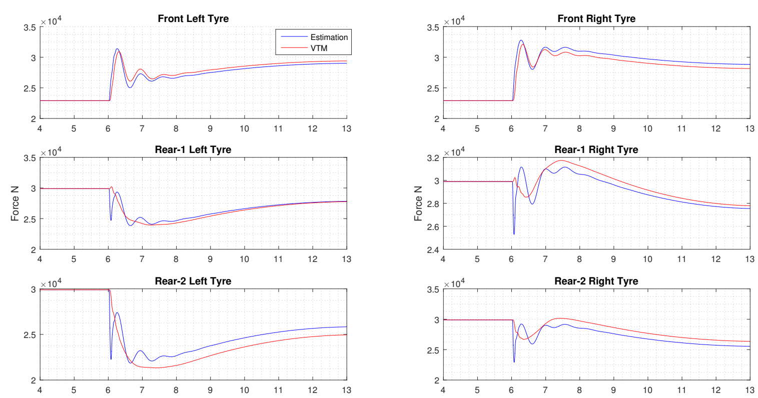

Figure 3.7: Scenario: Hard straight-line braking - Estimation of normal load forces on each wheel (blue line) compared to the normal load forces on each wheel from the VTM (red line)

Figure 3.7 shows normal load forces on each wheel. Figure 3.6 has spikes on estimations, which is blue line. Equations 14-19 have a_z in their denominator, hence when there is no acceleration on z-direction this term goes to infinity. In [2], they solve this problem by designing an observer, in figure 3.7 these terms (with a_z on the denominator) have been removed. There is no spikes in figure 3.7 compared to the figure 3.6.

3.3.5 Soft steered braking

Soft steered braking is considered as braking with ∼0.9 m/s^2 deceleration with a steering angle of 0.03 radian to the steering wheel. This test is done to see that the estimator reacts correctly when pitch motion and roll motion is presented. Figure 3.8 shows the acceleration in x-, y- and z-direction. There is a higher acceleration in y-direction due to the steering angle. Lateral acceleration will cause significant change in lateral load transfer and roll angle.

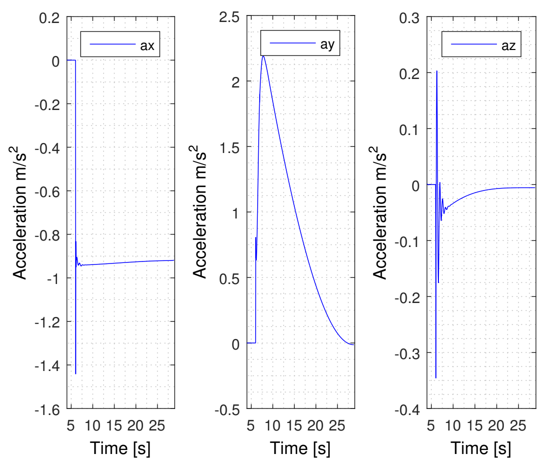

Figure 3.8: Acceleration in x-, y- and z-direction during steered braking

Figure 3.9 shows the result of the estimation algorithm. Estimation has spikes at the beginning of turn and braking because of the initial acceleration in z-direction.

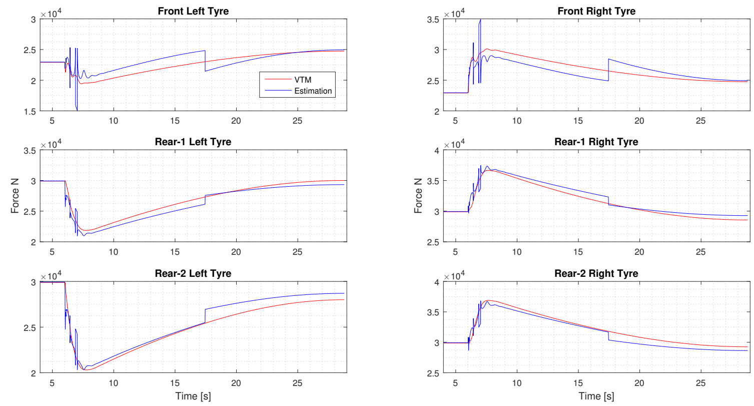

Figure 3.9: Scenario: Soft Steered Braking - Estimation of normal load forces on each wheel (blue line) compared to the normal load forces on each wheel from the VTM (red line)

Figure 3.9 shows the normal load forces on each wheel. The estimator shows no significant offset compared to the VTM in steady state but in transition response there are difference between estimation and the VTM. The discontinuity at 17 seconds is due to a sign change in a_z. From figure 3.9, it can also be seen that the load of the front axle is increasing and the load on the rear axles are decreasing, which is reasonable.

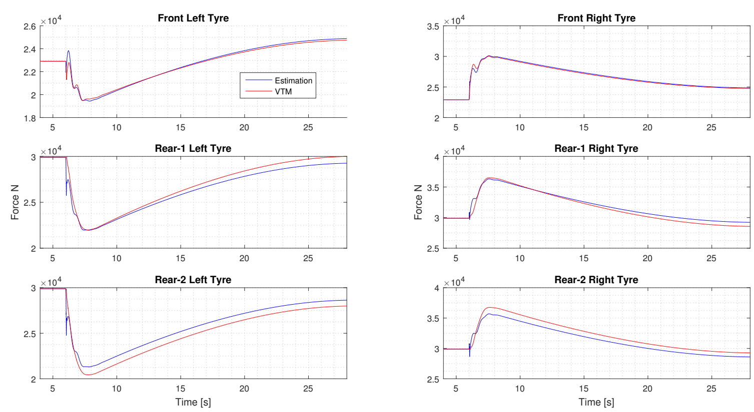

Figure 3.10: Scenario: Soft Steered Braking - Estimation of normal load forces on each wheel (blue line) compared to the normal load forces on each wheel from the VTM (red line)

Results are improved by neglecting the a_z term in denominator in equations

14-19, as is shown in figure 3.10 has much smoother results compared to 3.9.

3.3.6 Hard steered braking

Hard steered braking is considered as braking with 3 m/s^2 deceleration with a steering angle input of 0.03 radian. This test is done to see that the estimator reacts correctly when both pitch and roll motion is added. Figure 3.11 shows the acceleration in x-, y- and z-direction. There is an acceleration in y-direction due to the steering angle. It will cause significant lateral load transfer.

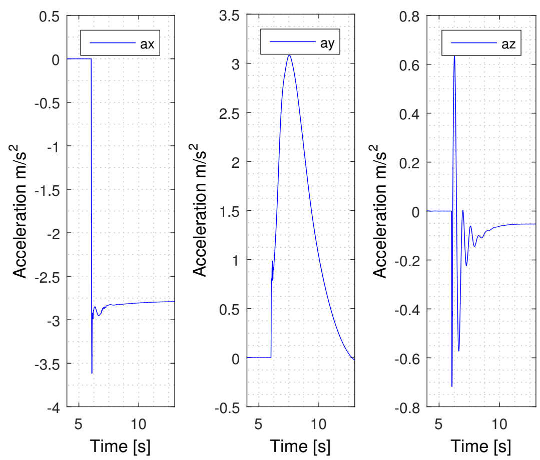

Figure 3.11: Acceleration in x-, y- and z-direction during steered braking

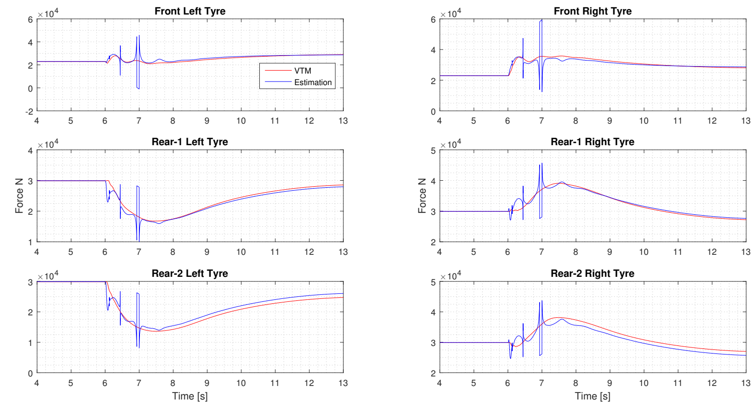

Figure 3.12: Scenario: Hard Steered Braking - Estimation of normal load forces on each wheel (blue line) compared to the normal load forces on each wheel from the VTM (red line)

Figure 3.12 shows the normal load forces on each wheel when in-turn with a hard braking. It causes both roll motion and pitch motion. Due to these motions, longitudinal and lateral load transfer can be observed in figure 3.12. The estimator shows no significant offset compared to the VTM in steady state, which indicates that the estimation algorithm is working correctly. The vehicle brakes at 6 seconds, after that oscillations can be seen in figure 3.12 due to changes in a_z. Nevertheless, the error in steady state is almost zero.

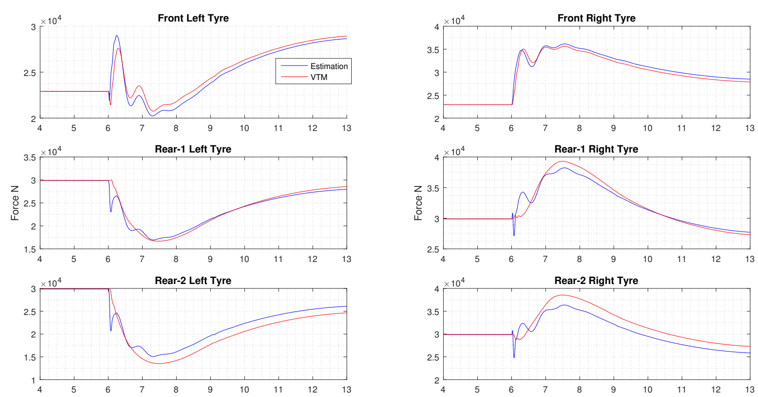

Figure 3.13: Scenario: Hard Steered Braking - Estimation of normal load forces on each wheel (blue line) compared to the normal load forces on each wheel from the VTM (red line)

Figure 3.13 shows the normal load forces on each wheel when in-turn with the terms containing a_z on the denominator in equation 14-19 removed. The spikes seen in figure 3.12 can be seen to be removed in figure 3.13.

4 Control Theory and Design

In this chapter, control theory and design will be introduced.

4.1 Control Theory

The following chapter will elaborate control theory and control design of the thesis. Firstly, background of control allocation is described, a solution of the optimization problem is then presented. Secondly, control allocation formulation is given for the 6x4 truck. Lastly, simulation results are represented.

4.2 Control Allocation

The following chapter will present the control allocation theory which is studied in [8].

4.2.1 Background

If the system is over-actuated, control allocation is an effective method for handling the actuators. Control allocation is different from the regulation task in the controller design. For example, if the task is to control the vehicle speed in the x-direction, the control allocator can be provided with two different actuators. A state equation for this example is given as:

$$\dot{x} = u_1 + u2 \tag{38}$$

where x is state variable which represents the vehicle speed on x-direction and u_1 and u_2 are control inputs. Equation 38 can be written as:

$$v = u_1 + u_2 \tag{39}$$

where v represents the virtual control input for the system. To reach the desired speed of the vehicle, u_1 and u_2 can be selected in many ways. The selection of the control inputs weights are called a control allocation problem.

Control allocation is a prevalent topic in different industries such as aerospace, marine, and vehicle industry. In the aerospace industry, researchers have done many studies about controlling roll, yaw and pitch angles [12]. In the marine industry, heading of the ship is done with a combination of different thrusters. Examples in the vehicle industry include yaw control of the vehicle, which is controlled by varying the brake forces on the wheels [13]. In heavy vehicles, the cruise control can be controlled by the engine torque and brake systems [14]. These examples show that control allocation is mainly about distributing requests to the actuators.

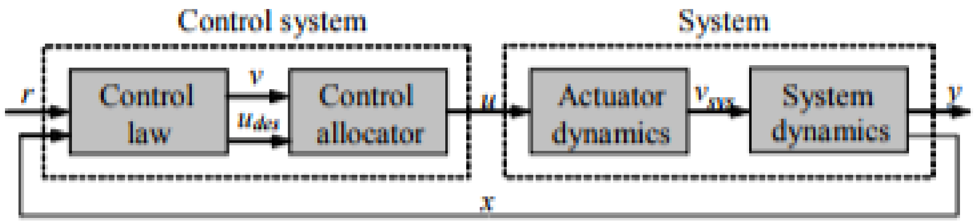

Figure 4.1: Control allocation structure is presented [1].

Figure 4.1 shows the control allocation structure. The figure shows us mainly two part: a control system and a plant. The control system has two blocks, which is control law and control allocator. The input of the control allocator is $\mathbf{v}$, the virtual control vector. The output of the control allocator is $\mathbf{u}$, the control signal for the actuators.

More specifically, the control part of the system is combining the two methods. The first task is to design a regulator for the system which depends on the control signal, such as voltage, current, torque, force, or similar. The last step of the control part is the allocation part which maps the control signals into the actuators.

General state space formulation of the dynamic system is formulated as:

$$\dot{\mathbf{x}} = f(\mathbf{x}, \mathbf{u}) \tag{40}$$

where $\mathbf{x} \in^n$ represents the dynamic of the system, $\dot{\mathbf{x}}$ is the derivative of the states, $\mathbf{u} \in^m$ is the control inputs of the system. This form can be written as:

$$\dot{\mathbf{x}} = g(\mathbf{x}) + h(\mathbf{x})\mathbf{u} \tag{41}$$

$$\dot{\mathbf{x}} = g(\mathbf{x}) + B\mathbf{u} \tag{42}$$

where $g(.)$ and $h(.)$ are nonlinear functions. $B \in^{nxm}$ is the control efficiency matrix which maps the control signals to actuators. If $m > n$, it means that the control inputs are more than controlled states and that it currently is an over-actuated system. An over-actuated system gives the flexibility of the allocator to control the states using different combinations of actuators. Equation 42 can be written as:

$$\dot{\mathbf{x}} = g(\mathbf{x}) + \mathbf{v} \tag{43}$$

where $\mathbf{v} \in^n$ is called virtual control input. $\mathbf{v}$ is the vector, which is an abstract of the real system. In this case [1], the number of controlled states is equal to that of the virtual inputs.

4.2.2 Optimization

Optimization is the second step of the control allocation problem. Optimization problem gives the unique **u** signals for the system. Equation 44 finds the optimum **u** signals. It is defined as:

$$\mathbf{u} = \underset{argmin}{\mathbf{u} \in \Omega} ||W_u(\mathbf{u} - \mathbf{u}_d)||_2^2 \tag{44}$$

where $\mathbf{u}_d$ is desired actuator vector.
The aim of the control allocator is to create a virtual vector and map it to **u** control signals. The second step of the optimization problem is given as:

$$\Omega = \underset{argmin}{\underline{\mathbf{u}} \leq \mathbf{u} \leq \overline{\mathbf{u}}} ||W_v(B\mathbf{u} - \mathbf{v})||_2^2 \tag{45}$$

where $\underline{\mathbf{u}}$ and $\overline{\mathbf{u}}$ are the actuator limitations.
Equations 44 and 45 have weighting matrices W_v and W_u. The weighting matrices distributes the control signals to the desired inputs. Limits of **u**, the control signals, keeps the solution in reasonable results. The actuator limit and rates is defined as:

$$\mathbf{u}_{min} \leq \mathbf{u} \leq \mathbf{u}_{max} \tag{46}$$

$$\Delta\mathbf{u}_{min} \leq \dot{\mathbf{u}} \leq \Delta\mathbf{u}_{max} \tag{47}$$

The optimization problem is solved by using Weighted Least Square(WLS) problem method. In WLS method, γ is a parameter introduced as a design parameter. If the design parameter γ is selected too large, the system can go into instability region. Therefore, it should be selected in a reasonable region. The optimization problem with all parameters is defined as:

$$\mathbf{u} = \underset{argmin}{\underline{\mathbf{u}} \leq \mathbf{u} \leq \overline{\mathbf{u}}} [||W_u(\mathbf{u} - \mathbf{u}_d)||_2^2 + \gamma ||W_v(B\mathbf{u} - \mathbf{v})||_2^2] \tag{48}$$

4.3 Controller Design

In this section, firstly, vehicle applications of control allocation is presented. The most common approach is defined in this section. Controlling the global forces on x- and y-direction and controlling the yaw moment are described with **u** vector, actuators, and $B - matrix$. In next section, **v**, the virtual vector, is extended by adding the M_y, pitch moment. The aim of it is to reduce the roll motion of vehicle in critical situations. An updated $B - matrix$ and **u** vector is given in this section. The following section gives information about controlling the M_x, the roll moment, with updated $B - matrix$. For the optimization problem, actuator constraints should be defined according to their capabilities which are given in next section. The final section presents simulation results with different test cases.

4.3.1 Background of control allocation in vehicle application

Control allocation is used in the avionics, marine, and road vehicle industries. Avionics and marine industry has a larger budget for developing their control systems. Hence, the studies seen in the literature have been applied mostly in these industries [15].

Heavy vehicles have over-actuated systems for motion control. In literature, there are many motion control studies about using control allocation technique, see [1]. The virtual control vector consists of the sum of F_x forces, the sum of F_y forces and the sum of moments in the z-direction. Virtual control vector is given as:

$$\mathbf{v} = \begin{bmatrix} \sum_i F_{x,i} \\ \sum_i F_{y,i} \\ \sum_i M_{z,i} \end{bmatrix} \equiv \begin{bmatrix} \mathbb{F}_x \\ \mathbb{F}_y \\ \mathbb{M}_z \end{bmatrix} \tag{49}$$

The $\mathbf{u}$ vector is defined as:

$$\mathbf{u} = \begin{bmatrix} Tb_{fl} & Tb_{fr} & Tb_{r1l} & Tb_{r1r} & Tb_{r2l} & Tb_{r2r} & Tb_{tag} & M_{eng} & Steer_f & Steer_r \end{bmatrix} \tag{50}$$

where Tb_{ij} are the individual brake torque requests, M_{eng} is the engine torque, $Steer_f$ and $Steer_r$ present the steering angles of the first axle and steered tag axle respectively.
The control efficiency matrix is defined, $B - matrix$, as:

$$B = \begin{bmatrix} \frac{1}{R_e} & \frac{1}{R_e} & \frac{1}{R_e} & \frac{1}{R_e} & \frac{1}{R_e} & \frac{1}{R_e} & \frac{2}{R_e} & \frac{1}{R_e} & 0 & 0 \\ 0 & 0 & 0 & 0 & 0 & 0 & 0 & 0 & 2C\alpha & 2C\alpha \\ -\frac{E_1}{2R_e} & \frac{E_1}{2R_e} & -\frac{E_2}{R_e} & \frac{E_2}{2R_e} & \frac{E_3}{2R_e} & \frac{E_3}{2R_e} & 0 & 0 & 2C\alpha l_1 & -2C\alpha l_3 \end{bmatrix} \tag{51}$$

where R_e is the radius of the wheel, E_1, E_2 and E_3 is the track width of the truck.

4.3.2 Pitch control

The aim is to keep the pitch motion of the truck at a reference of the road angle. The virtual control vector is updated by adding a new row to it. $\mathbb{M}_y$ is the global moment in the y-direction. The $\mathbf{v}$ virtual control vector is defined as:

$$\mathbf{v} = \begin{bmatrix} \sum_i F_{x,i} \\ \sum_i F_{y,i} \\ \sum_i M_{z,i} \\ \sum_i M_{y,i} \end{bmatrix} \equiv \begin{bmatrix} \mathbb{F}_x \\ \mathbb{F}_y \\ \mathbb{M}_z \\ \mathbb{M}_y \end{bmatrix} \tag{52}$$

In this case, the $\mathbf{u}$ matrix is modified by adding the suspension actuators.

$Sus_i,\ i = fl, fr, r_1l, r_1r, r_2l, r_2r$ is defined as suspension pressures produced from air suspension system.

The VTM has three suspensions. One is in the middle of the front axle, and the other two is on the middle point of the rear axles. Hence, the forces are added before sending into the VTM. The volume of the suspension is controlled by the pressure.

These equations are now for the 6x4 vehicle. The new control vector, $\mathbf{u}$, is defined as:

$$\mathbf{u} = \begin{bmatrix} Tb_{fl} & Tb_{fr} & Tb_{r1l} & Tb_{r1r} & Tb_{r2l} & Tb_{r2r} & Tb_{tag} & M_{eng} & Steer_f & \cdots \\ \cdots & Steer_r & Sus_{front} & Sus_{Rear} \end{bmatrix} \tag{53}$$

Equation 53 is modified to include 16 actuators. The modified control vector is given as:

$$\mathbf{u} = \begin{bmatrix} Tb_{fl} & Tb_{fr} & Tb_{r1l} & Tb_{r1r} & Tb_{r2l} & Tb_{r2r} & Tb_{tag} & M_{eng} & Steer_f & \cdots \\ \cdots & Steer_r & Sus_{Fl} & Sus_{Fr} & Sus_{R1l} & Sus_{R1r} & Sus_{R2l} & Sus_{R2r} \end{bmatrix} \tag{54}$$

Equation 54 presents new actuator vector. The difference from equation 53 is that the truck has only two suspension system where the front wheels are controlled via single pressure control channel and same with the rear.

Equation 55 has four rows; the last row is added to $B - matrix$ since the aim is to control the pitch angle of the vehicle using the suspension actuators.

$$B = \begin{bmatrix} \frac{1}{R_e} & \frac{1}{R_e} & \frac{1}{R_e} & \frac{1}{R_e} & \frac{1}{R_e} & \frac{1}{R_e} & \frac{2}{R_e} & \frac{1}{R_e} & 0 & \cdots \\ 0 & 0 & 0 & 0 & 0 & 0 & 0 & 0 & 2C_\alpha & \cdots \\ -\frac{E_1}{2R_e} & \frac{E_1}{2R_e} & -\frac{E_2}{2R_e} & \frac{E_2}{2R_e} & -\frac{E_3}{2R_e} & \frac{E_3}{2R_e} & 0 & 0 & 2C_\alpha l_1 & \cdots \\ 0 & 0 & 0 & 0 & 0 & 0 & 0 & 0 & 0 & \cdots \end{bmatrix}$$
$$\begin{bmatrix} \cdots & 0 & 0 & 0 & 0 & 0 & 0 & 0 \\ \cdots & 2C_\alpha & 0 & 0 & 0 & 0 & 0 & 0 \\ \cdots & 2C_\alpha l_3 & 0 & 0 & 0 & 0 & 0 & 0 \\ \cdots & 0 & -l_1 A_{bellow} & -l_1 A_{bellow} & l_2 A_{bellow} & l_2 A_{bellow} & l_3 A_{bellow} & l_3 A_{bellow} \end{bmatrix} \tag{55}$$

4.3.3 Roll control

The aim is to keep the roll motion of the truck at the reference of the road angle when the truck is turning and braking. M_x is added to the virtual vector. Errors in roll angle are controlled by the suspension.

The $B - matrix$ is updated to include the influence of air suspension pressure on the roll moment M_x.

$$B = \begin{bmatrix} \frac{1}{R_e} & \frac{1}{R_e} & \frac{1}{R_e} & \frac{1}{R_e} & \frac{1}{R_e} & \frac{1}{R_e} & \frac{2}{R_e} & \frac{1}{R_e} & 0 & \cdots \\ 0 & 0 & 0 & 0 & 0 & 0 & 0 & 0 & 2C_\alpha & \cdots \\ -\frac{E_1}{2R_e} & \frac{E_1}{2R_e} & -\frac{E_2}{2R_e} & \frac{E_2}{2R_e} & -\frac{E_3}{2R_e} & \frac{E_3}{2R_e} & 0 & 0 & 2C_\alpha l_1 & \cdots \\ 0 & 0 & 0 & 0 & 0 & 0 & 0 & 0 & 0 & \cdots \end{bmatrix}$$
$$\begin{bmatrix} \cdots & 0 & 0 & 0 & 0 & 0 & 0 & 0 \\ \cdots & 2C_\alpha & 0 & 0 & 0 & 0 & 0 & 0 \\ \cdots & 2C_\alpha l_3 & 0 & 0 & 0 & 0 & 0 & 0 \\ \cdots & 0 & -E_1 A_{bellow} & E_1 A_{bellow} & -E_2 A_{bellow} & E_2 A_{bellow} & E_3 A_{bellow} & E_3 A_{bellow} \end{bmatrix} \tag{56}$$

4.3.4 Pitch and roll control

Previously, work is done by first controlling the pitch, and later only roll angle is controlled. The suspension vectors are now updated for controlling roll and pitch at the same time. The new virtual vector with global moment of the pitch and global moment of the roll is defined as:

$$\mathbf{v} = \begin{bmatrix} \sum_i F_{x,i} \\ \sum_i F_{y,i} \\ \sum_i M_{z,i} \\ \sum_i M_{y,i} \\ \sum_i M_{x,i} \end{bmatrix} \equiv \begin{bmatrix} \mathbb{F}_x \\ \mathbb{F}_y \\ \mathbb{M}_z \\ \mathbb{M}_y \\ \mathbb{M}_x \end{bmatrix} \tag{57}$$

The updated $B-matrix$ is defined as:

$$B = \begin{bmatrix} \frac{1}{R_e} & \frac{1}{R_e} & \frac{1}{R_e} & \frac{1}{R_e} & \frac{1}{R_e} & \frac{1}{R_e} & \frac{2}{R_e} & \frac{1}{R_e} & 0 & \cdots \\ 0 & 0 & 0 & 0 & 0 & 0 & 0 & 0 & 2C_\alpha & \cdots \\ -\frac{E_1}{2R_e} & \frac{E_1}{2R_e} & -\frac{E_2}{2R_e} & \frac{E_2}{2R_e} & -\frac{E_3}{2R_e} & \frac{E_3}{2R_e} & 0 & 0 & 2C_\alpha l_1 & \cdots \\ 0 & 0 & 0 & 0 & 0 & 0 & 0 & 0 & 0 & \cdots \\ 0 & 0 & 0 & 0 & 0 & 0 & 0 & 0 & 0 & \cdots \end{bmatrix}$$
$$\begin{bmatrix} \cdots & 0 & 0 & 0 & 0 & 0 & 0 & 0 \\ \cdots & 2C_\alpha & 0 & 0 & 0 & 0 & 0 & 0 \\ \cdots & 2C_\alpha l_3 & 0 & 0 & 0 & 0 & 0 & 0 \\ \cdots & 0 & -l_1 A_{bellow} & -l_1 A_{bellow} & l_2 A_b ellow & l_2 A_{bellow} & l_3 A_{bellow} & l_3 A_{bellow} \\ \cdots & 0 & -E_1 A_{bellow} & E_1 A_{bellow} & -E_2 A_{bellow} & E_2 A_{bellow} & E_3 A_{bellow} & E_3 A_{bellow} \end{bmatrix} \tag{58}$$

4.3.5 Constraints

A truck has different actuators for different tasks. For example, if a driver wants the truck to move in the x-direction, the driver can use the engine for producing torque in the x-direction. When the truck is on a downhill, it is sufficient to use foundation brakes or engine brakes to maintain the speed. In another case, when the truck is doing a maneuver, it uses its steering angle to make a turn. Another case, when it comes to a gravel road, the truck uses its suspensions to keep the pitch angle and road comfort stable. All these cases are done by actuators. Actuators have limited capacity. These limits will be constraints for the optimization problem.

- **Friction Braking**
  The friction brakes at the wheels does not give positive torque to the truck since braking does not produce positive energy for the system, so maximum braking torque is $Tb, i = 0\ Nm$, which is the brake system on each wheel.

  On the other hand, when the truck is braking, it generates negative torques. The braking system has a capacity of smaller torque than currently chosen, but for this study minimum torque is chosen for each wheel as $Tb, i = -10000\ Nm$.

- **Engine Torque**
  Main torque producer for the truck is the engine. An engine of a truck can be used in both ways, for accelerating and decelerating the truck. The engine of the truck has a capacity of producing higher torque for acceleration and less torque for deceleration than chosen. However, for this study, maximum engine torque is chosen as $Teng_{max} = 20000\ Nm$ and minimum engine torque is chosen as $Teng_{min} = -1000\ Nm$.

- **Steering**
  The purpose of giving a steering angle is to make a turn. A truck can steer more than this constraint, but for this study, steering is limited for the truck as $\pm 0.15\ radians$.

- **Suspension Pressure**
  The suspension actuators are controlled by pressure. The suspension system has a pressure capacity and is limited. The truck has on suspension actuators for each wheels.

  The minimum pressure values for the front suspensions are $P_{front,i} = 0$ Pascal $i = front_{left}$ and $front_{right}$. The minimum pressure values for the rear suspensions are $P_{rear,i} = 0$ Pascal $i = rear, j_{left}$ and $front, j_{right}$. $j = 1, 2$. j presents the driven axle 1 and driven axle 2.

  The maximum pressure values for the front suspensions are $P_{front,i} = 1000000$ Pascal $i = front_{left}$ and $front_{right}$. The maximum pressure values for the rear suspensions are $P_{rear,i} = 1000000$ Pascal $i = rear, j_{left}$ and $front, j_{right}$. $j = 1, 2$. j presents the driven axle 1 and driven axle 2.

4.4 Control Allocator Simulation

The following section presents the test case for testing and validating the control allocator. Test is done using Volvo's VTM Simulink model with an initial speed of 15 m/s in a dry road conditions. The inlet valve to each suspension actuator is modelled with an 8 mm orifice, and a step response with a change of 5 bars.

4.4.1 Test cases for the control allocator

There are 3 test scenarios for the testing control allocator structure. The first test is to validate that the pitch control is working, which is done by testing the control allocator in a hard straight-line braking event with and without feedback for the roll. The second test carried out is a steered hard braking but disabling feedback of the pitch and only control the roll. The third test is done by giving feedback of pitch and roll during a steered hard braking event. Afterward, the simulations are repeated with ideal suspension control valves (e.g. very large inlet valves), resulting in the desired flowrate being instantly reached. Only the first test which does not include feedback for the roll is left out. Finally, the maximum pressure of the air suspension system is increased with 25% and tested with the ideal flowrate model.

4.4.2 Hard straight-line braking pitch control

M_y is calculated using the following equation:

$$M_y = a_x * h_{cg} * m + P * (\theta_{ref} - \theta_{act}) + \int (I * \theta_{ref} - \theta_{act}) + D * \frac{\partial(\theta_{ref} - \theta_{act})}{\partial t} \quad (59)$$

where P, I, and D are tuning parameters for a PID controller, θ_{ref} is a reference pitch angle and θ_{act} is an actual pitch angle. The requested acceleration for the hard straight-line braking event and the reached acceleration in x- and y-direction are shown below.

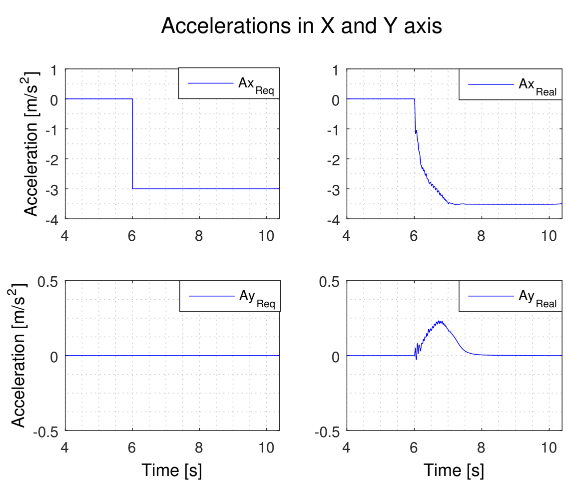

Figure 4.2: Acceleration in x- and y-direction during hard straight-line braking

In the figure, it is visible that the reached acceleration in the x-direction is more than the requested acceleration. This could be due to the constants in the control allocator and the VTM. The straight-line braking is resulting in a small amount of lateral acceleration, but it is insignificant.

Favorable results have been obtained during simulations, where the pitch angle of the vehicle would normally go to a steady state value, now goes to zero. Roll angle graphs have also been added to make sure that the roll is still within reasonable limits. The results of the simulations are plotted and shown in figure 4.3.

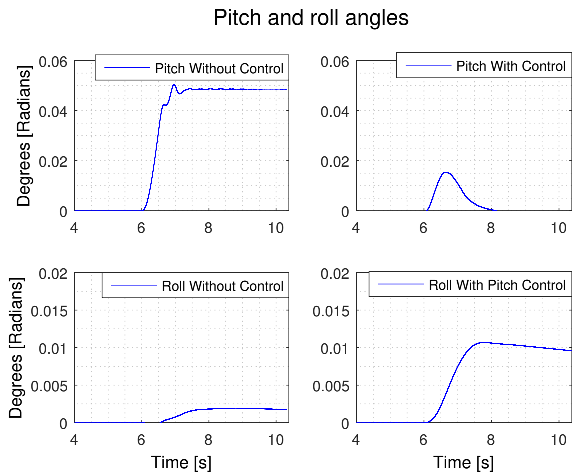

Figure 4.3: Roll and Pitch angles

The requested pressures are shown in figure 4.4, while the reached suspension pressures are shown in figure 4.5. If we compare the requested pressures, the achieved suspension pressure, and the pitch angle figures, it is visible that when the pitch angle increases the requested pressures increase on the front suspensions and decrease on the rear. When the achieved suspension pressure starts to change, and the pitch angle starts to drop and gets closer to zero, the pressure requests are also dropping to keep it steadily around zero. This is one verification of many that the control allocator is doing what it is supposed to do.

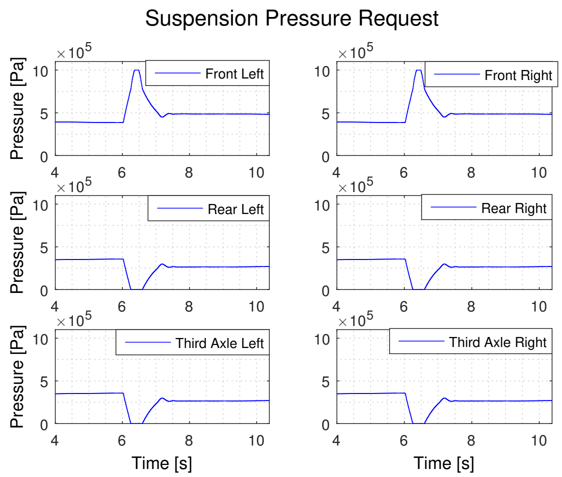

Figure 4.4: Requested suspension pressure

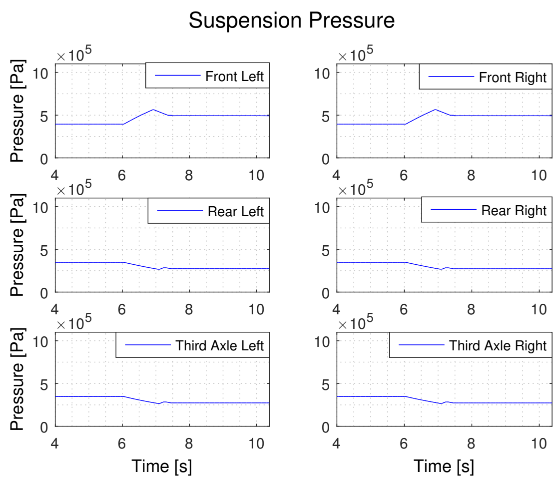

Figure 4.5: Achieved suspension pressure

4.4.3 Hard straight-line braking pitch control ideal

Under the same test condition, but assuming that the flowrate to the bellows is equal to the desired flowrate instantly. The requested pressure is shown in figure 4.6 and the achieved pressure in figure 4.7.

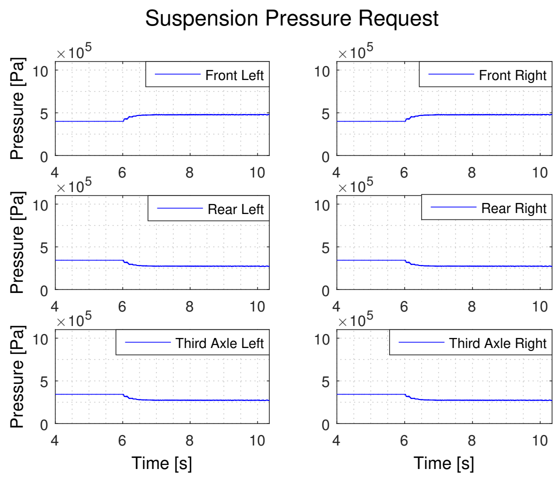

Figure 4.6: Requested suspension pressure

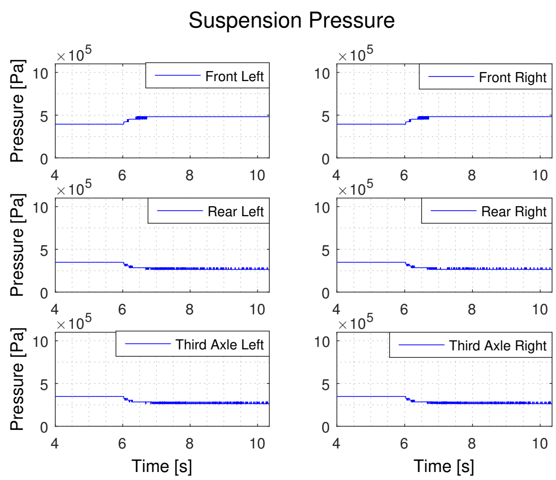

Figure 4.7: Achieved suspension pressure

The requested acceleration for the hard straight-line braking and the reached acceleration in x- and y-direction are shown below.

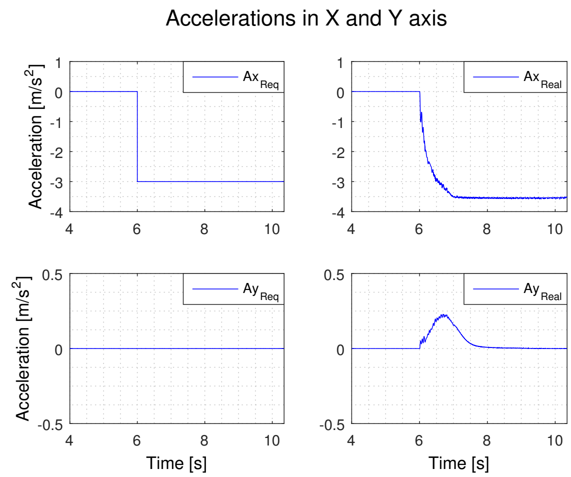

Figure 4.8: Acceleration in x- and y-direction during hard straight-line braking

The acceleration is shown again to make sure the scenario remains the same and is not changed since the comparison with the non-ideal would not be valid anymore. The figure 4.8 validate that the scenario remains the same.

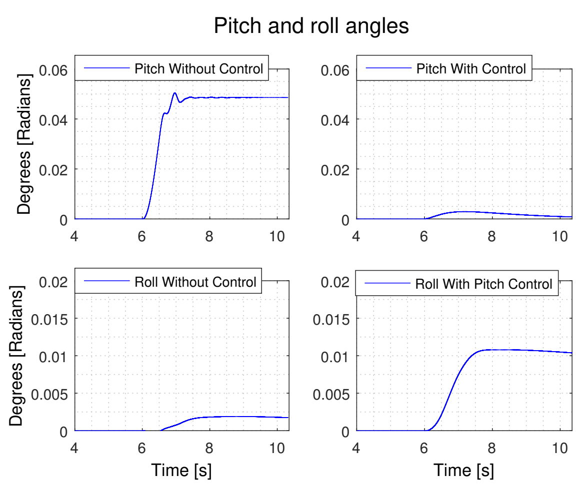

Figure 4.9: Roll and Pitch angles

When the flowrate is ideal, the maximum pitch is five times lower and is shown in figure 4.9. This is due to the bellow reacting much quicker than currently possible with air suspension systems. This also shows that if a faster suspension than air suspension is mounted, the result can achieve much better results. The maximum pressure limit was however not changed, it is possible that a suspension with higher limits will also achieve better results if the flowrate is quick enough.

4.4.4 Hard straight-line braking combined pitch & roll control

A feedback loop is now added for M_x and is calculated through the equation:

$$M_x = a_y * h_{cg} * m + P * (\phi_{ref} - \phi_{act}) + \int I * (\phi_{ref} - \phi_{act}) + D * \frac{\partial(\phi_{ref} - \phi_{act})}{\partial t} \tag{60}$$

where P, I, and D are tuning parameters for a PID controller, ϕ_{ref} is a reference roll angle and ϕ_{act} is an actual roll angle The requested acceleration for the steered hard braking event and the reached acceleration in x- and y-direction are shown below.

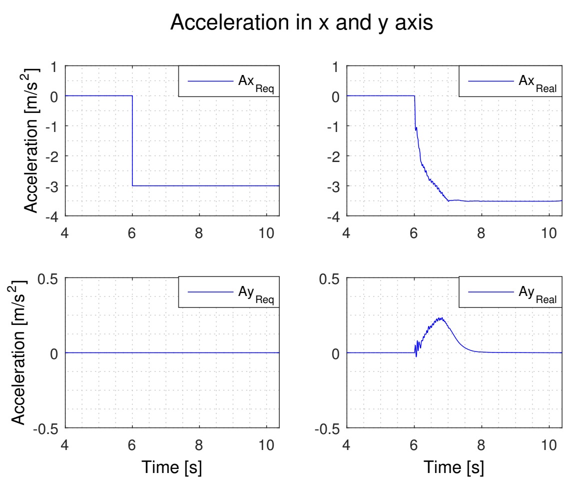

Figure 4.10: Acceleration in x- and y-direction during steered hard braking

In figure 4.11 the roll and pitch angle has been improved, but the pitch angle does not return to zero. The reason could be that the control allocator is still trying to improve the roll angle since the error is much larger there and hence some compromise between roll and pitch angle must be made.

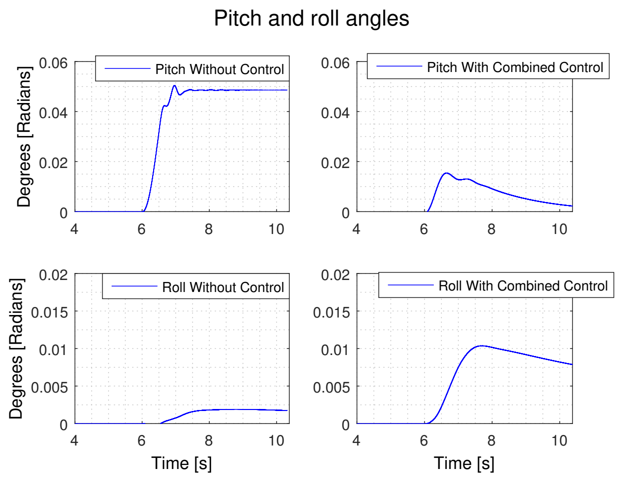

Figure 4.11: Roll and Pitch angles

From the figure 4.12, the control allocator is using front left and rear right suspensions to change the roll angle while using front right and rear left suspensions to change the pitch angle. Since the required pressure change for pitch is lower, it is also easier achievable. However, since the roll requires a higher pressure change, it takes longer time as visible in figure 4.13.

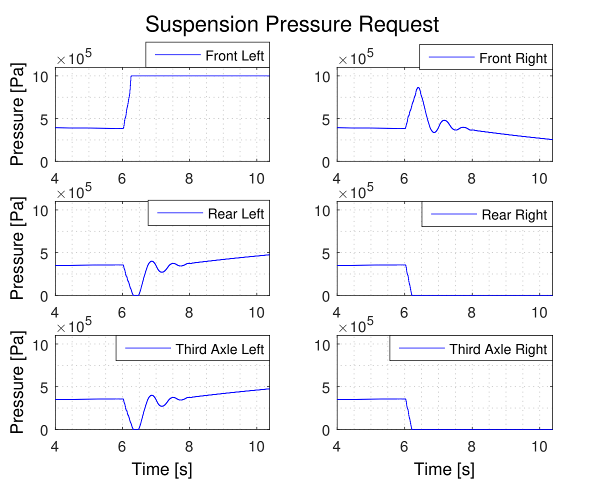

Figure 4.12: Requested suspension pressure

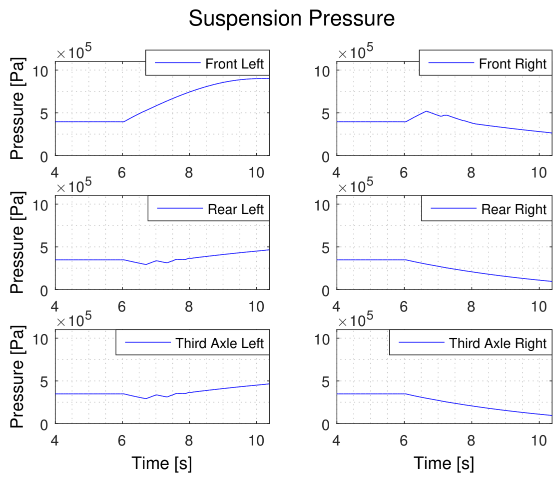

Figure 4.13: Achieved suspension pressure

4.4.5 Steered hard braking roll control

The feedback of M_y is given as zero and M_x is calculated through the equation 60. The requested acceleration for the steered hard braking and the reached acceleration in x- and y-direction are shown below.

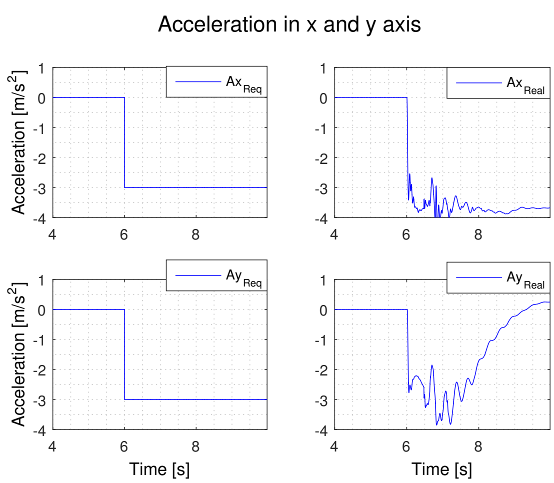

Figure 4.14: Acceleration in x- and y-direction during steered hard braking

In figure 4.15 the roll angle has been improved, but the air suspension is too slow, and the pressure limits are too low. The pitch angle is not controlled but plotted in the figure to make sure it does not reach unreasonably high or low limits. The control allocator pressure requests are in the figure 4.16, and clearly shows that the control allocator is instantly trying to reach the maximum and minimum limits of the suspensions. However, the airflow and the limits of the stiffness restricts the control allocator from better performing, as visible in figure 4.17.

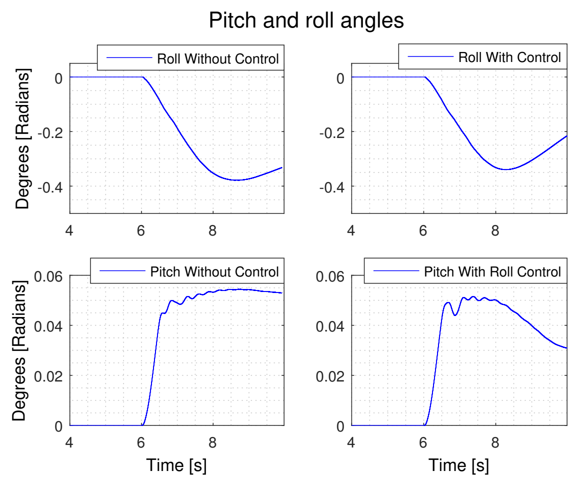

Figure 4.15: Roll and Pitch angles

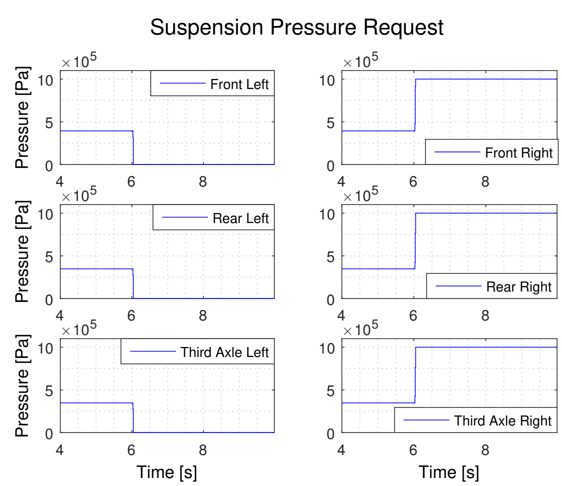

Figure 4.16: Requested suspension pressure

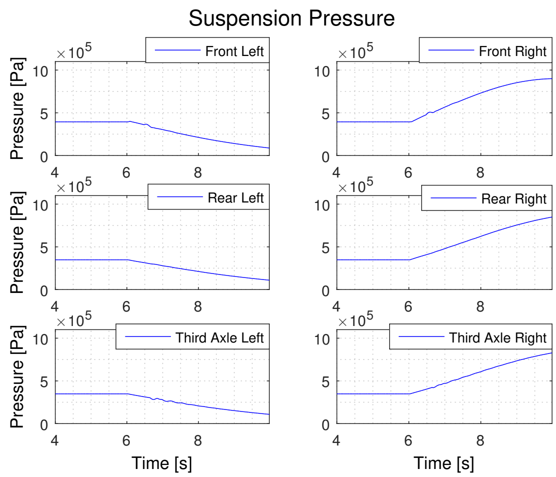

Figure 4.17: Achieved suspension pressure

4.4.6 Steered hard braking roll control ideal

This is the same scenario as above, but assuming that the flowrate to the bellows is equal to the desired flowrate instantly as visible between the requested pressure in figure 4.18 and achieved suspension pressure in figure 4.19.

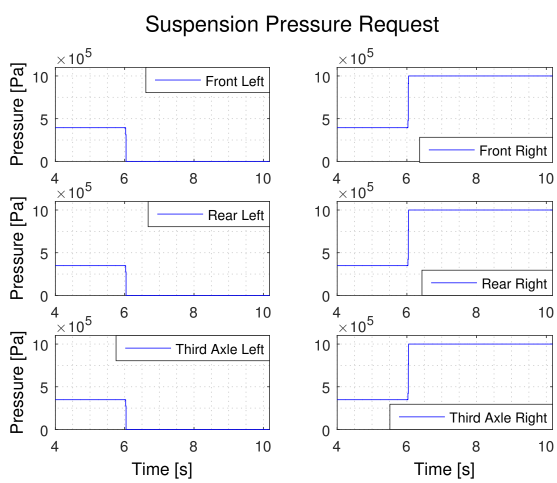

Figure 4.18: Requested suspension pressure

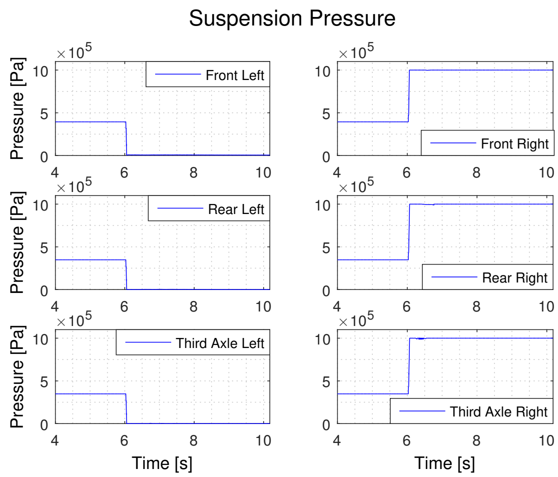

Figure 4.19: Achieved suspension pressure

The requested acceleration for the hard straight-line braking and the reached acceleration in x- and y-direction are shown below.

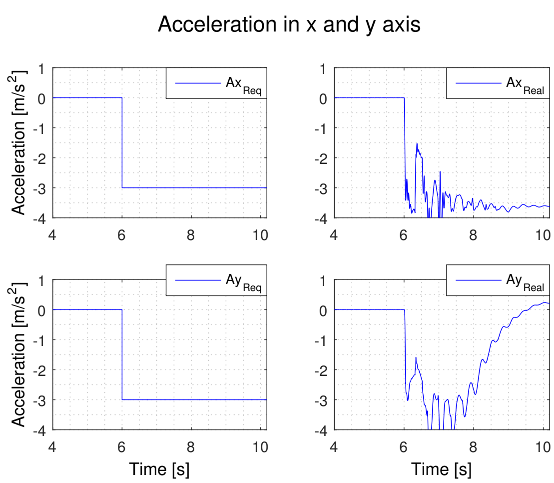

Figure 4.20: Acceleration in x- and y-direction during steered hard braking

The acceleration is shown again to make sure the scenario remains the same and is not changed since the comparison with the non-ideal would not be valid anymore. The figure 4.20 validate that the scenario remains the same.

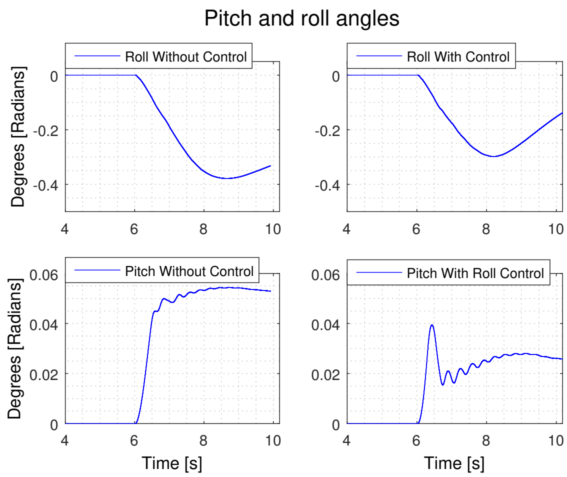

Figure 4.21: Roll and Pitch angles

When the flowrate is ideal, the roll is lower than previously. This shows that not only a faster suspension is needed, but also a suspension which has higher maximum pressure.

4.4.7 Steered hard braking combined pitch & roll control

This scenario considers feedback for M_y and M_x. The requested acceleration for the steered hard braking and the reached acceleration in x- and y-direction are shown below.

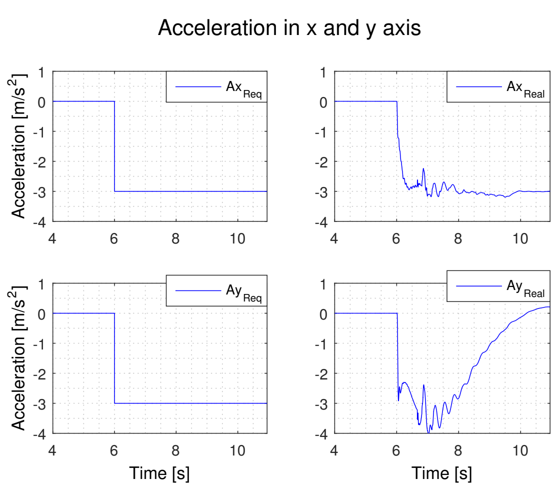

Figure 4.22: Acceleration in x- and y-direction during steered hard braking

In figure 4.23 the roll has been improved slightly while the pitch has improved more. This is probably due to the weighing matrix W_v, where the weight for pitch is double of the weight for the roll. The reason of this weighing is because the air suspensions are too slow and have too low maximum pressure to correct the roll error, but if we give the same weighing the pitch will also be corrected slowly while still having the same plot in roll angle. Hence, we have chosen to consider pitch control as of higher value than roll.

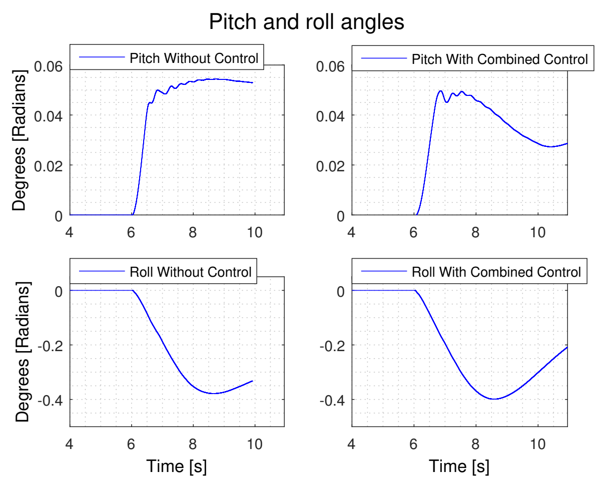

Figure 4.23: Roll and Pitch angles

When looking at the figure 4.24 it is visible that the control allocator prioritizes the roll angle more than the pitch angle since the roll angle error is much larger. Due to suspension limitations, and slow dynamics of air suspensions, the achieved suspension pressure takes time to build up to that pressure as shown in figure 4.25.

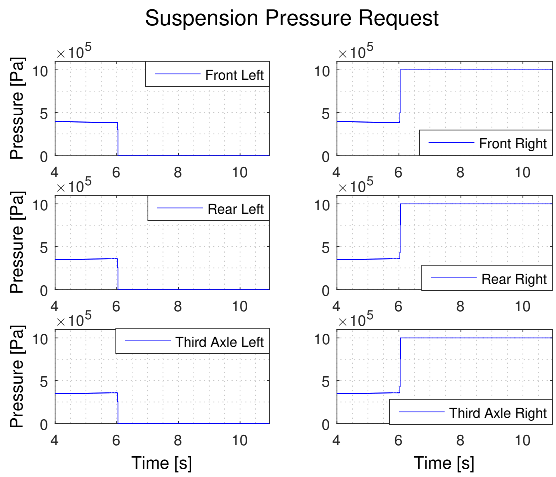

Figure 4.24: Requested suspension pressure

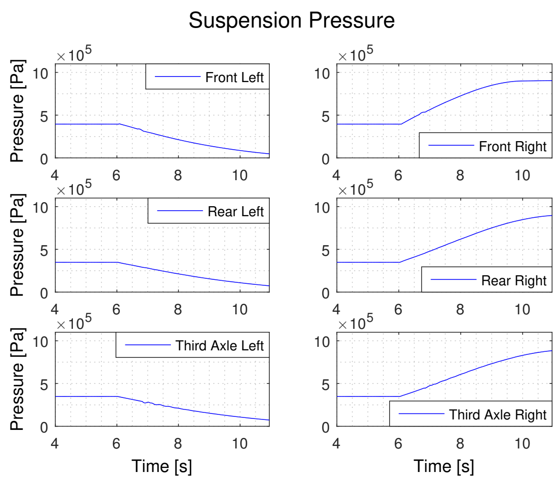

Figure 4.25: Achieved suspension pressure

4.4.8 Steered hard braking combined pitch & roll control ideal

This scenario is the same scenario as above but considers ideal flowrate. The requested pressure is shown in figure 4.26, while achieved pressure is in figure 4.27.

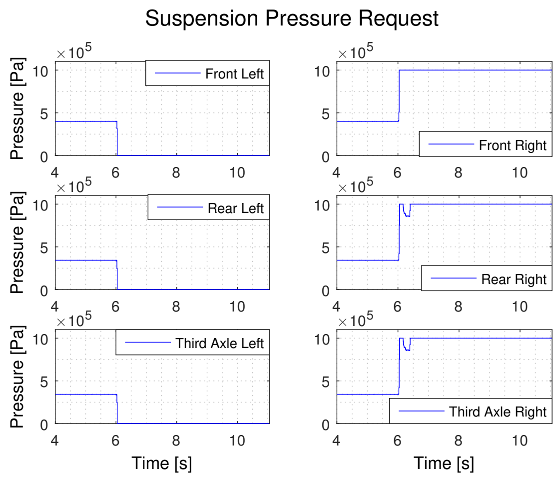

Figure 4.26: Requested suspension pressure

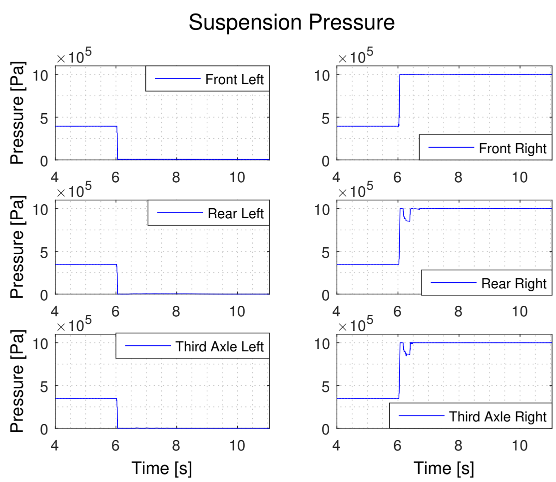

Figure 4.27: Achieved suspension pressure

Figure 4.26 and 4.27 have the same result since the test case is accepted as an ideal.
The requested acceleration for the steered hard braking and the reached acceleration in x- and y-direction are shown below.

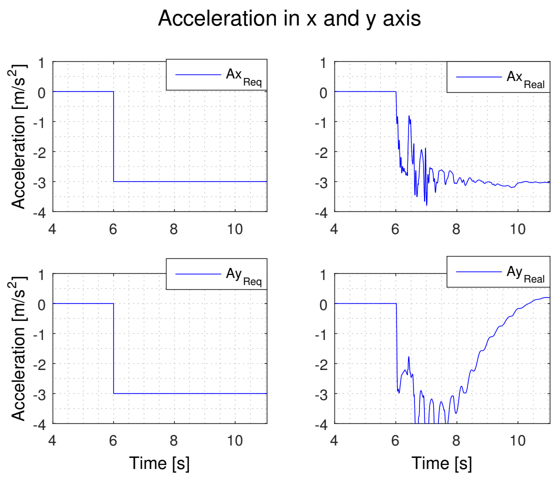

Figure 4.28: Acceleration in x- and y-direction during steered hard braking

In figure 4.29 the roll has been improved slightly while the pitch has improved more. The improvement of the pitch is not what the control allocator seeks for, but does it unintendedly. Since the total stiffness of the vehicle is increasing, the pitch angle is decreasing too. An ideal suspension offers more generous results, but could still be improved if the maximum pressure is increased.

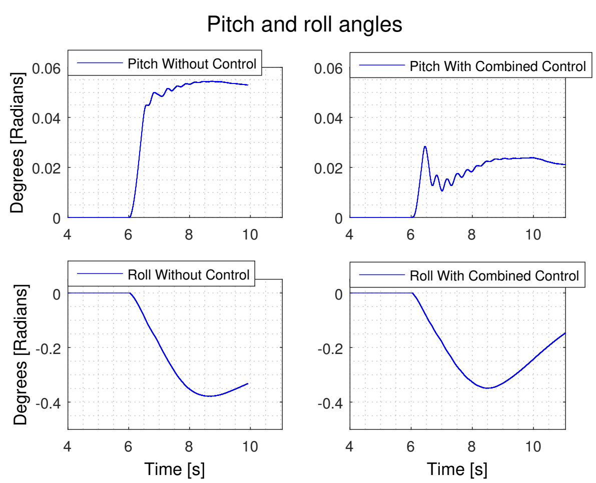

Figure 4.29: Roll and Pitch angles

4.4.9 Steered hard braking combined pitch & roll control ideal 120% P˙max

This scenario is the same scenario as above but considers ideal flowrate and increase of 20% in maximum pressure of the suspension bellow. The control allocator is still mainly trying to control the roll angle since the pressure request in figure 4.30 shows that it is trying to decrease the pressure in the left side and increasing in the right. Since it is an ideal suspension, the achieved suspension pressure in figure 4.31 is almost the same as the requested pressure.

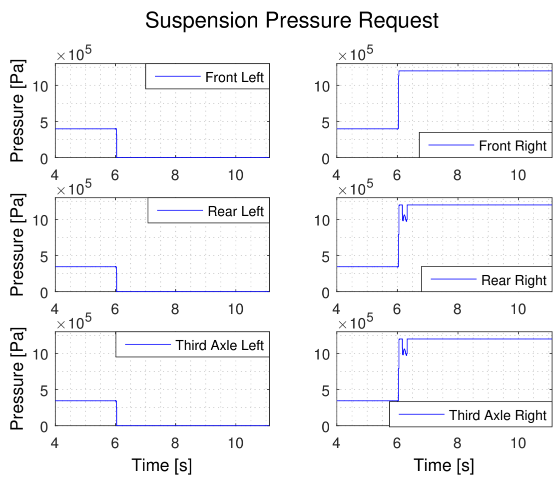

Figure 4.30: Requested suspension pressure

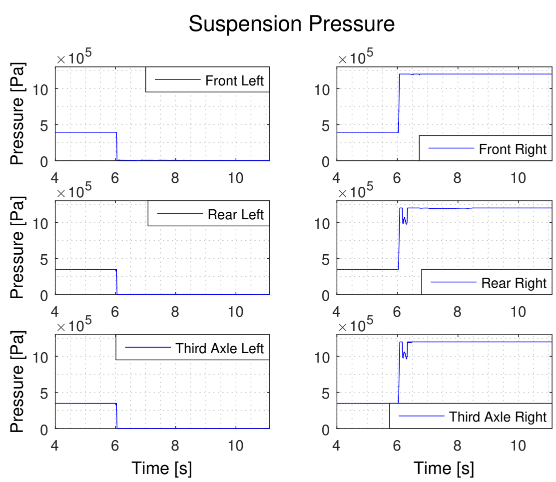

Figure 4.31: Achieved suspension pressure

The requested acceleration for the steered hard braking and the reached acceleration in x- and y-direction are shown below.

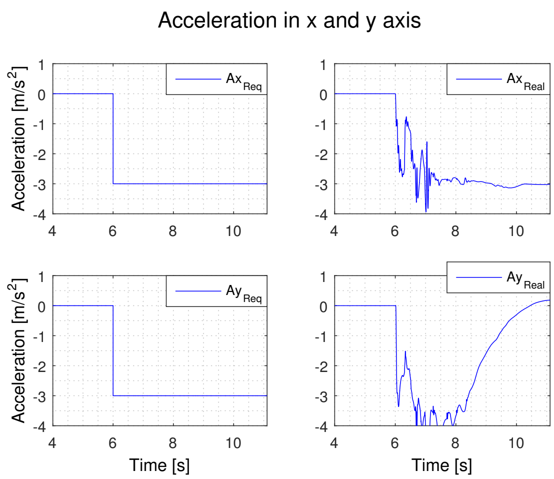

Figure 4.32: Acceleration in x- and y-direction during steered hard braking

In figure 4.33 the roll and the pitch has both improved significantly. This shows us that a faster suspension with higher stiffness possibilities can give significantly better results than previous simulations.

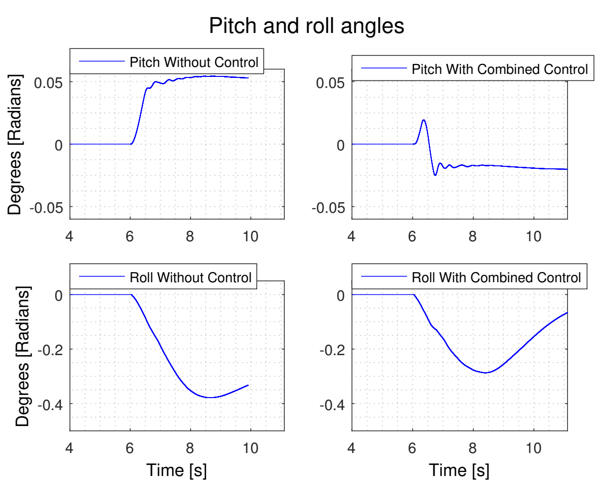

Figure 4.33: Roll and Pitch angles

4.5 Modified Control Allocator Simulation

Consultation with suspension engineers leads to the conclusion of outlet and inlet valve sizes being too small and has hence been increased to 20 mm.

4.5.1 Steered hard braking combined pitch & roll control

With the updated valve sizes, the scenario has been re-simulated. The graphs below can be compared to the graphs above with the same scenario:

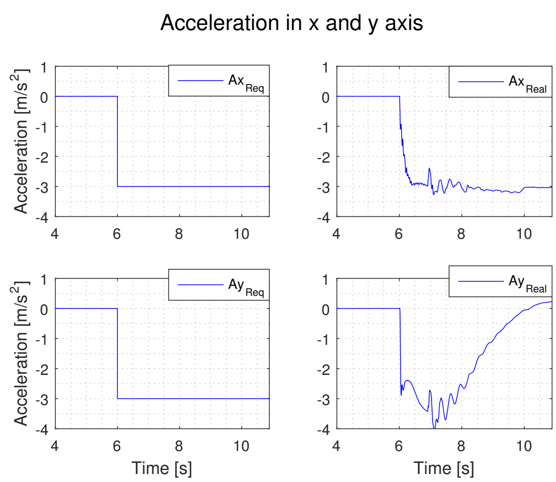

Figure 4.34: Acceleration in x- and y-direction during steered hard braking

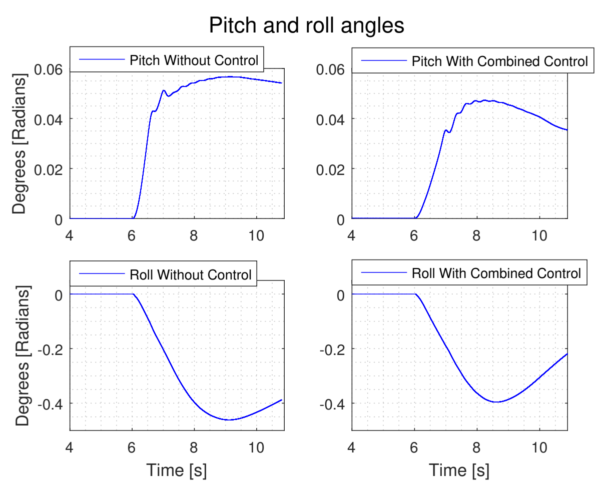

Figure 4.35: Roll and Pitch angles

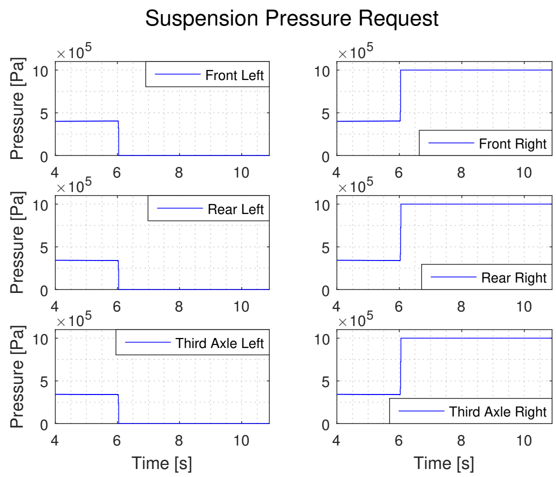

Figure 4.36: Requested suspension pressure

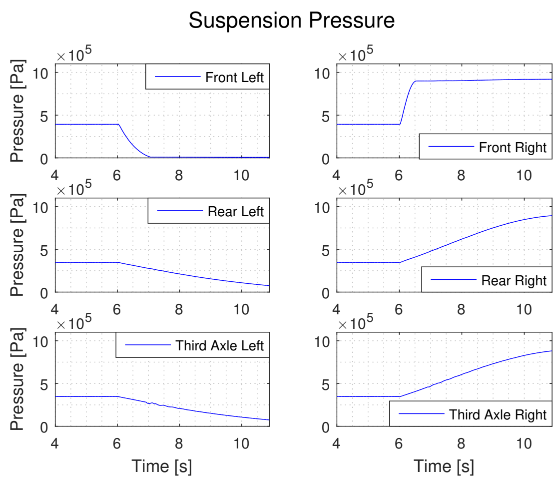

Figure 4.37: Achieved suspension pressure

Figure 4.35, 4.36 and 4.37 shows that increasing valve size improves the roll and pitch controller performance.

5 Conclusion

The two main objective of this thesis is to estimate the normal load forces on each wheel and to design a control allocator. The estimation algorithm and the control allocator is needed to control global forces on x and y-direction and to keep roll, yaw and pitch angle according to the reference. Increasing the stability of the vehicle and decreasing the stopping distance is crucial in many scenarios.

A method has been studied to estimate normal forces on each wheel. The method has been shown to be accurate during steady state but exhibited some unexpected spikes that need to be further investigated if the estimator is to be used in real life.

Pitch and roll motion has been added to an existing control allocator for a truck. It is clearly visible that the allocation successfully manages to keep the pitch and roll angles at the road angle. It keeps them closer to zero. During steered hard braking, the pressure of the bellow does not catch up with the pressure request until the end of the simulation. If a bellow with faster response is mounted, the results will clearly be better. For some scenarios, even faster bellows are not enough to maintain low roll angles. This is due to the limitations of the bellow supply pressure.

5.1 Discussion

Obviously, an infinitely quick bellow with infinite pressure capacity would be the best choice. Since the real world is not ideal and has limitations, this is not possible. But there are alternative suspensions, such as hydraulic suspensions or size-increasable bellow air suspensions, which take shorter time to reach the requested pressure. The size-increasable bellows are mainly used in buses, and is by definition able to increase or decrease in bellow size to decrease or increase the pressure together with the suspension height to give a faster response to the pressure request.

5.2 Future Work

The following section will present future work about the thesis.

5.2.1 Estimation

Estimation algorithms could be quite simple, as used in this thesis. For future studies, it would be better to have two separate models, in which one is the VTM model, to run parallel. This would remove some offsets, and if the other model matches the VTM model, it would be rather simple to implement Kalman Filter structures. Estimation would be more accurate if filters are implemented. It would also reduce the cost of the vehicle since implementing a filter and an observer for estimating the vehicle states would result in fewer sensors used. Eventually, this improvement will reduce the cost of the truck and make a more efficient system.

If z acceleration and position sensors were implemented on every tyre, the estimation would be greatly improved as shown in figure 5.1. The cost would increase compared to today's system, but with technology consistently growing and sensors getting cheaper, this solution may become feasible in the near future.

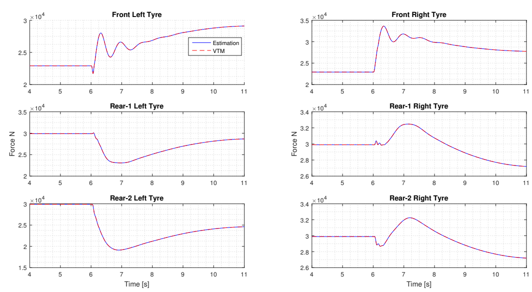

Figure 5.1: Scenario:Steered hard braking - Normal load forces on each wheel compared to sensor on every tyre (blue signal with dash) compared to the VTM model (red signal)

5.2.2 Actuator models

The current VTM model has only three suspension systems which are in the middle of the front axle and middle of the driven axles. This model could be extended to six individual suspension and joints to increase the possibilities for future control allocation problems.

The current suspension system in the truck is an air suspension. Air suspension systems have a larger delay than hydraulic suspensions. Instead of using air suspension, electrical or hydraulic suspension systems can be used for future trucks to remove long dead times. In addition to this, since each wheel has its own suspension system, height level control can easily be achieved by adding a single row to the $B\text{-}matrix$ with requested added pressure and adding a vertical force variable F_z in the virtual vector $\mathbf{v}$. The requested added pressure would be the pressure the control allocator wants to add on every tyre, by increasing the pressure the truck would increase in height and by lowering the pressure it would decrease in height.

6 Bibliography

References

[1] B.Källstrand (2016), Control Allocation for Vehicle Motion Control: Maximizing Traction and Steering Capabilities Under Different Road Conditions, Master's Thesis EX075/2016 , Chalmers University of Technology

[2] Kun Jiang, A. Pavelescu, A. Victorino and A. Charara, "Estimation of vehicle's vertical and lateral tire forces considering road angle and road irregularity," 17th International IEEE Conference on Intelligent Transportation Systems (ITSC), Qingdao, 2014, pp. 342-347. doi: 10.1109/ITSC.2014.6957714

[3] M. Doumiati, A. Victorino, A. Charara D. Lechner (2009) Lateral load transfer and normal forces estimation for vehicle safety: experimental test, Vehicle System Dynamics, 47:12, 1511-1533, DOI: 10.1080/00423110802673091

[4] M. Doumiati , A. Victorino , D. Lechner , G. Baffet A. Charara (2010) Observers for vehicle tyre/road forces estimation: experimental validation, Vehicle System Dynamics, 48:11, 1345-1378, DOI: 10.1080/00423111003615204

[5] Jia, Gang Li, Liang Cao, Dongpu. (2015). Model-Based Estimation for Vehicle Dynamics States at the Limit Handling. Journal of Dynamic Systems, Measurement, and Control. 137. 1-8. 10.1115/1.4030784.

[6] Yi, Kyongsu Yoon, Jangyeol Kim, Dongshin. (2007). Model-based Estimation of Vehicle Roll State for Detection of Impending Vehicle Rollover. 1624 - 1629. 10.1109/ACC.2007.4282507.

[7] G. Baffet, A. Charara, D. Lechner D. Thomas (2008) Experimental evaluation of observers for tire–road forces, sideslip angle and wheel cornering stiffness, Vehicle System Dynamics, 46:6, 501-520, DOI: 10.1080/00423110701493963

[8] Härkegård, O. (2003) Backstepping and Control Allocation with Applications to Flight Control. PhD Thesis, Linköping University, Sweden.

[9] Volvo Truck Model (2014), Simulink library developed at Volvo Group Trucks Technology, Department BF72991.

[10] Bengt J H Jacobson, Vehicle Dynamics Compendium for Course MMF062; edition 2016

[11] Leon Henderson. Improving emergency braking performance of heavy goods vehicles. PhD thesis, University of Cambridge, 2014.

[12] Durham, W.C., 1993. Constrained control allocation. J.Guid. Control Dynam., 16(4): 717-725.

[13] Kiencke, U. and Nielsen, L., Automotive Control Systems for Engine, Driveline and Vehicle, SAE International, ISBN 0-7680-0505-1,2000

[14] D. Axehill, J. Sjöberg, Adaptive cruise control for heavy vehicles—hybrid control and MPC, Master's thesis, Linköpings universitet, February 2003

[15] L. Laine, "Reconfigurable motion control systems for over-actuated road vehicles," Ph.D. dissertation, Department of Applied Mechanics, Chalmers University of Technology, SE-412 96 Goteborg, Sweden, June 2007.

7 Appendix

7.1 Noisy Data Simulation in VTM

In this test case, noises are added to sensors of the VTM to get more realistic results compared to previous cases.

7.1.1 Noisy data simulation for Method 1 soft straight-line braking

The second test case is done with similar conditions except deceleration is chosen as 0.9 m/s^2. Without filtering, estimation results are noisy. Hence, the noisy signals are sent through a filter, which gives better results.

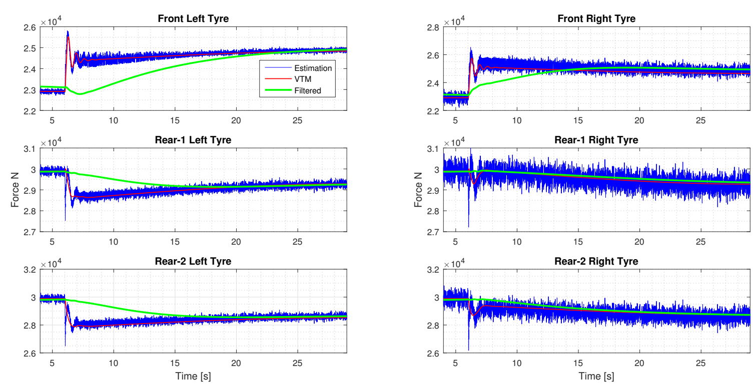

Figure 7.1: Scenario: Soft Line Braking - Estimation of normal load forces on each wheel (blue line) compared to the normal load forces on each wheel from the VTM (red line) and filtered estimation of normal load forces on each wheel (green line)

Figure 7.1 shows the normal forces on each wheel with the VTM, estimation result and filtered estimation result. The estimator has oscillations due to noisy signals and it does not compensate the oscillations. Due to oscillations, butterworth filter is used to remove oscillation but filtered response is quite slow in the beginning. During steady state, filtered response catches the VTM.

7.1.2 Noisy data simulation for Method 1 hard straight-line braking

Hard straight-line braking test has 3 m/s^2 deceleration with zero steering input. In figure 7.2, green line shows the filtered estimation signal.

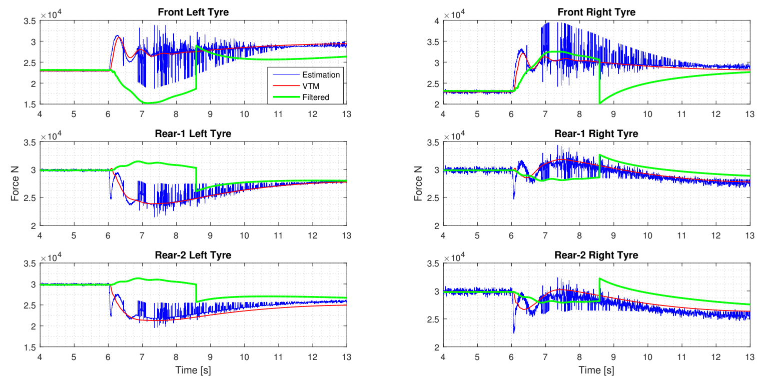

Figure 7.2: Scenario: Hard Line Braking - Estimation of normal load forces on each wheel (blue line) with compared to the load forces on each wheel from the VTM (red line) and filtered estimation of normal load forces on each wheel (green line)

Figure 7.2 shows the normal forces on each wheel with the VTM, estimation result and filtered estimation result. The estimator has oscillations due to hard braking and noisy signals. To improve the estimation, butterworth filter is used. Green line represents the improved result but still it is not satisfying since transient response is very slow. But in steady state it catches the VTM.

7.1.3 Noisy data simulation for Method 1 soft steering braking

The truck is slowing down with 0.9 m/s^2 deceleration with 0.03 radian steering angle. Using the previous filter, noise is removed from estimation results. Figure 7.3 shows the normal forces on each wheel with the VTM, estimation result and filtered estimation result. The green line represents the filtered results of the test. The graph shows that estimation does not work very well in noisy conditions.

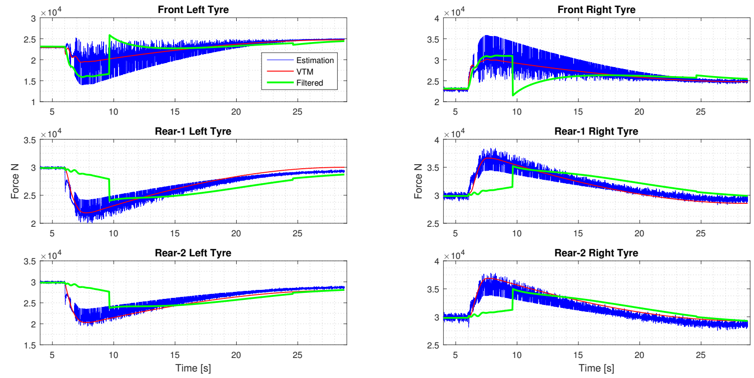

Figure 7.3: Scenario: Soft Turn Braking - Estimation of normal load forces on each wheel (blue line) compared to the normal load forces on each wheel from the VTM (red line) and filtered estimation of normal load forces on each wheel (green line)

7.1.4 Noisy data simulation for Method 1 hard steering braking

The truck has 3 m/s^2 deceleration and 0.03 radian steering angle after six seconds. Figure 7.4 shows the normal forces on each wheel with the VTM, estimation result and filtered estimation result. Estimation result is not satisfying, hence butterworth filter is applied to the estimation to improve the estimation of normal force on each wheel. Green line represents the filtered response. It is much better than without filter.

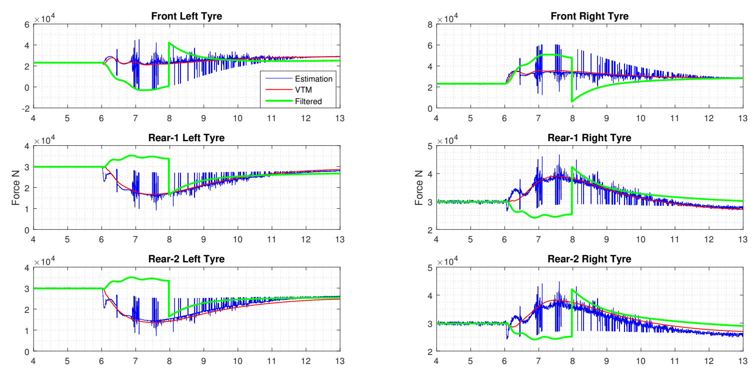

Figure 7.4: Scenario: Hard Turn Braking - Estimation of normal load forces on each wheel (blue line) with compared to the load forces on each wheel from the VTM (red line) and filtered estimation of normal load forces on each wheel (green line)